This is the peer-reviewed, final accepted version for American Mineralogist, published by the Mineralogical Society of America.
The published version is subject to change. Cite as Authors (Year) Title. American Mineralogist, in press.
DOI: https://doi.org/10.2138/am-2020-7452. http://www.minsocam.org/

Revision 5

Word count: 7520

Thermodynamic characterization of synthetic lead-arsenate apatites with different halogen substitutions

Bartosz Puzio[1*], Lei Zhang[2], Jennifer E.S. Szymanowski[2], Peter C. Burns[2,3], Maciej Manecki[1]

[1]AGH University of Science and Technology, Department of Mineralogy, Petrography and Geochemistry, al. Mickiewicza 30, 30-059 Kraków, Poland (*correspondence: bpuzio@agh.edu.pl; tel.: +48-732-845-422)

[2]Department of Civil and Environmental Engineering and Earth Sciences, University of Notre Dame, Notre Dame, IN 46556, USA

[3]Department of Chemistry and Biochemistry, University of Notre Dame, Notre Dame, IN 46556, USA

This is the peer-reviewed, final accepted version for American Mineralogist, published by the Mineralogical Society of America.
The published version is subject to change. Cite as Authors (Year) Title. American Mineralogist, in press.
DOI: https://doi.org/10.2138/am-2020-7452. http://www.minsocam.org/

ABSTRACT

Thermodynamic parameters have been measured for synthetic analogs of the mimetite-group minerals $Pb_5(AsO_4)_3X$ (X = OH, Cl, Br, I) belonging to the apatite supergroup. Phases precipitated from aqueous solutions under ambient conditions with well-characterized structures and compositions were studied. For each phase, dissolution enthalpy was experimentally determined by oxide melt drop solution calorimetry in the molten solvent of sodium molybdate ($3Na_2O{\cdot}4MoO_3$) at 976 K. The enthalpy of formation from the elements $\Delta H°_{f,el}$ was calculated using thermochemical cycles and was −3030.6 ± 11.5, −3026.6 ± 15.8, −2967.6 ± 25.0, and −2993.1 ± 12.2 kJ/mol for $Pb_{5.00}(AsO_4)_{3.00}OH_{0.86}(CO_3)_{0.07}$, $Pb_{5.00}(AsO_4)_{3.00}Cl_{0.80}(CO_3)_{0.10}$, $Pb_{5.00}(AsO_4)_{3.00}Br_{0.80}(CO_3)_{0.10}$, and $Pb_{5.00}(AsO_4)_{3.00}I_{0.45}OH_{0.35}(CO_3)_{0.10}$, respectively. These $\Delta H°_{f,el}$ values exhibit typical trends for apatites: they increased (were less negative) with the increasing molar mass and ionic radius of X and decreased with the electronegativity and ionization energy of X. The compilation and comparison of data for Ca-, Pb-, P-, and As-apatites revealed correlations indicating that thermodynamic enthalpic stability is largely influenced by chemical factors (e.g., differences in electronegativities of the elements, ionization energy, or ionic characteristics of the bonds) and to a lesser extent by physical and geometric parameters in the crystal structure related to the mass and size of the X anion. Using the correlations, it was possible to estimate the value of hitherto unknown $\Delta H°_{f,el}$ for $Pb_5(AsO_4)_3F$, −3144.3 ± 66.5 kJ/mol. The observed relationships apply to the entire apatite supergroup and can be used to predict the values of $\Delta H°_{f,el}$ for phases that have not been studied experimentally. The new data on environmentally significant phases will contribute to the modeling of mineral-water interactions, particularly for potential use in the remediation of soils and wastes contaminated with Pb and As and in the immobilization of radioactive waste containing ^{129}I.

Keywords: Lead apatite, lead arsenates, calorimetry, enthalpy, mimetite, iodoapatites

INTRODUCTION

Pyromorphite $Pb_5(PO_4)_3Cl$ and mimetite $Pb_5(AsO_4)_3Cl$ are the most stable lead apatites in the environment (Manecki 2019). With the capacity to hold more than half of the long-lived radioactive elements of the periodic table in its structure (Hughes and Rakovan 2015) and a structure that allows both cationic and anionic solid solutions and substitutions, apatite is also a versatile material for application in the field of environmental remediation (Rakovan and Pasteris 2015). The formation of these minerals in contaminated areas of mine dumps significantly reduces Pb and As bioavailability and improves ecosystem health (e.g., Nriagu 1974; Comba 1987; Ruby et al. 1994; Laperche et al. 1997; Manecki et al. 2006, 2019; Chappell and Scheckel 2007; Karna et al. 2018). Apatites are also used in permeable reactive barriers (PRBs), e.g., to isolate groundwater from radionuclides or as a form of processed waste in planned nuclear waste repositories (Conca et al. 2000; Rigali et al. 2016).

The thermodynamic stability of pyromorphite has been extensively studied (see, e.g., Nriagu 1974; Manecki 2006; Manecki et al. 2009 and the literature therein). However, little is known about the thermodynamic properties of mimetite-group minerals. To date, only one study has reported calculations of the enthalpy of formation for $Pb_5(AsO_4)_3Cl$ from dissolution experiments (Bajda 2010). No calorimetric measurements have been reported to date. In addition, there are no thermodynamic data for other phases in this group where Cl is replaced by OH, F, Br, or I, and general information on these phases is scarce (Flis et al. 2011; Cao et al. 2014). This limits understanding of the properties of apatite as a group and prevents the thermodynamic modeling of mineral-water interactions in Pb- and As-bearing systems of high environmental importance (Twidwell et al. 1994; Liu et al. 2009; Nordstrom et al. 2014; Topolska et al. 2014).

The synthetic analogs of apatites have been of interest to environmental mineralogists and materials science engineers for decades. Attempts to synthesize and characterize mimetites with various halide substitutions were made as early as 1959 (Merker and Wondratschek 1959). Currently, research on iodine varieties has become particularly important because of their ability to incorporate radioactive fission products such as I-129 and Cl-36 (Lei et al. 2020). The immobilization of I-129, one of the problematic fission products, has been particularly challenging in high-level waste (HLW) disposal because of its high toxicity and volatility as well as its very long half-life (Cohen 1977). Unlike most liquid wastes, iodine evolves primarily as a gas during reprocessing and cannot be properly incorporated into borosilicate glass, which is the ultimate destination of most liquid wastes. Regardless of the waste form, the ultimate goal is to dispose of these I-129-containing materials underground in deep geologic repositories and isolate them from human activities for long periods. Therefore, many waste forms have been proposed to adequately capture the iodine content of waste streams (Sava et al. 2012; Ma et al. 2014; Jie et al. 2017). Among the most promising materials developed to date, synthetic apatites, a group of synthetic analogs of mineral wastes inspired by natural apatites, are a promising option because of their high thermal and chemical stability and radiation resistance.

A series of lead arsenate apatite-like phases $Pb_5(AsO_4)_3X$ (where X = OH, Cl, Br, and I) have been synthesized and used to determine the effect of X anions on enthalpic stability. These well-characterized synthetic analogs of mimetite were used in high-temperature solution calorimetric studies to derive their standard heats of formation. The new $\Delta H°_{f,el}$ data enabled aggregation and comparison of the thermodynamic data for a broad range of Ca to Pb of P and As apatites with different substitutions at position X. Existing thermodynamic data estimation approaches (Drouet 2015; Glasser 2019) were used to calculate $\Delta H°_{f,el}$ for mimetites for comparison with the new calorimetric data.

EXPERIMENTAL METHODS

Synthesis

The following four phases are isostructural with arsenate-lead apatite (mimetite) and were synthesized using a modified method reported by Baker (1966): $Pb_5(AsO_4)_3OH$, $Pb_5(AsO_4)_3Cl$, $Pb_5(AsO_4)_3Br$, and $Pb_5(AsO_4)_3I$. The apatites were synthesized by the dropwise addition of aqueous solutions of $Pb(NO_3)_2$, $Na_2HAsO_4{\cdot}7H_2O$, and NH_4X (where X = Cl, Br, and I). Unlike calcium apatites, lead arsenate apatites do not incorporate significant amounts of Na, and the use of sodium salts in synthesis does not result in the appearance of detectable amounts of Na in the structure (Bajda 2010, Huang et al. 2014, Sordyl et al. 2020). The Pb/As and As/X (where X = OH, Cl, Br, and I) molar ratios in the mixed solutions were maintained at 1.67 and 3.00, respectively. All samples were synthesized at 298.15 K open to the air (in the presence of CO_2), making the procedure relevant to the environmental conditions. $Pb_5(AsO_4)_3Cl$ and $Pb_5(AsO_4)_3Br$ were synthesized at a pH of 4.5 to obtain a homogeneous product and avoid formation of schultenite $PbHAsO_4$ at lower pH. $Pb_5(AsO_4)_3OH$ and $Pb_5(AsO_4)_3I$ precipitated at pH 6. Higher pH can cause the formation of lead hydroxide. The solutions (prepared with double distilled water) were added at a rate of 2 mL/min, and the pH was maintained using a 1 M solution of NH_4OH or HNO_3. After the synthesis, the suspensions were aged for 72 h, centrifuged, washed with double distilled water, and dried in an oven at 378.15 K for 48 h.

Characterization of solids

An aliquot of 50 mg of each sample was completely dissolved in 100 mL of 0.02 M EDTA (dissolved in 10% HNO_3) solution and analyzed for Pb and As using inductively coupled plasma–optical emission spectrometry (ICP–OES) (Perkin Elmer Optima 7300DV) and for Br and I using ICP–MS (iCAP RQ (C2) Thermo Scientific). C, H, and N were measured by CHNS

analysis using a Vario EL III (Elementar GmbH) apparatus with a TCD detector. Solid characterization with scanning electron microscopy (SEM) was performed at a low vacuum for uncoated samples using an FEI Quanta 200 FEG scanning electron microscope (Hillsboro, OR, USA) equipped with secondary electron (SE) and backscattered electron (BSE) detectors. Energy dispersive spectrometry (EDS, FEI Quanta) was used to monitor variations in chemical composition. Powder X-ray diffraction (XRD) patterns were recorded using a Rigaku SmartLab diffractometer (Neu-Isenburg, Tokyo, Japan) with graphite-monochromatized CuKα radiation at an operating voltage of 45 kV, a current of 200 mA, a step size of 0.02°, and a counting time of 1 s/step. The phases were identified using the ICCD database and XRAYAN software (Marciniak et al. 2006). Raman spectra were recorded by a DXR Raman microscope (Thermo Fisher Scientific) using 10 000 scans at 2 cm^{-1} with an Nd laser YAG at 520 nm. Powders were analyzed directly without preparation. The laser power was maintained at 10 mW. The maxima and decomposition of the Raman spectrum bands were determined with mixed Gaussian–Lorentzian functions using OMNIC software.

High-temperature oxide melt solution calorimetry

A high-temperature Setaram AlexSys 1000 was used to measure the drop solution enthalpies of synthetic halogenated mimetites. The samples were dissolved in the molten solvent sodium molybdate ($3Na_2O{\cdot}4MoO_3$) at 976 K. The calorimeter was calibrated against a heat content of ~5 mg of α-Al_2O_3. The instrument, calorimetric experiment, and calorimeter calibration are described elsewhere in detail (Navrotsky 1977, 1997, 2014; Shvareva et al. 2012). Silica crucibles were used in the present study, as they were found to provide consistent data similar to platinum crucibles (Zhang et al. 2018). A semi-micro balance was used to weigh approximately 5

This is the peer-reviewed, final accepted version for American Mineralogist, published by the Mineralogical Society of America.
The published version is subject to change. Cite as Authors (Year) Title. American Mineralogist, in press.
DOI: https://doi.org/10.2138/am-2020-7452. http://www.minsocam.org/

mg of powdered samples, which were then hand-pressed into pellets of 1.5 mm in diameter. High-purity O_2 was used to remove any water in the headspace of the calorimetric setup, which would have resulted from the dissolution of $Pb_5(AsO_4)_3OH_{0.86}(CO_3)_{0.07}$ or $Pb_5(AsO_4)_3I_{0.45}OH_{0.35}(CO_3)_{0.10}$ in the sodium molybdate solvent. Seven to eleven drop solution experiments were performed for each material to ensure the reproducibility of the measurements (see Supplemental[1] Tables S1–S4). Errors associated with calorimetric analyses are reported as two standard deviations of the mean and are less than 4% of the reported values of the drop solution enthalpies (see Supplemental[1] Tables S1–S4). To complete the calculation of thermochemical cycles, the enthalpies of the drop solution for KCl and KBr were determined experimentally by using the same instrument before the analysis of synthetic apatite-like phases (see Supplemental[1] Tables S5–S6). Tables with thermochemical cycle data are included below.

To determine potential loss of volatile Cl, Br or I during calorimetry, an additional ex-situ experiment was performed. Portions of 35 mg of KCl, KBr and KI were mixed with 9.5 g of sodium molybdate solvent ($3Na_2O$-$4MoO_3$), weighed and placed in an oven at 976 K. The samples were heated for 45 min and then quenched, cooled in a desiccator, and reweighed. Quenched solvent-fused KCl was visually homogeneous. The measured mass loss of 1.35 mg is much lower than the quantity of Cl in the sample (16.47 mg). We assume that all of the KCl has remained in the solvent and that the small mass loss is due to moisture. In contrast, the solidified KBr alloy had dark beige spots, which may indicate the formation of a heterogeneous melt. When the KBr experiment was repeated at 1023 K, the final product appeared homogeneous. It is therefore likely that at the temperature of the calorimetric measurements (976 K) the KBr reagent did not form a homogeneous alloy with molybdate. In the case of the KI sample, purple gas was noted during quenching of the sample, but the resulting alloy was visually homogeneous. The measured mass loss of 27.82 mg was nearly equal to the expected loss of 26.6 mg that would

result if all I was degassed. The small excess of 1.22 mg is similar to that observed for KCl and is likely due to moisture content. These results indicate that Cl was completely retained in the melt, Br was partially lost, and I was completely removed during calorimetry.

The above statements were further confirmed using in situ thermogravimetric analysis coupled with analysis of evolved gases and ex situ SEM/EDS. A TA Discovery (TA Instruments, USA) coupled to a quadrupole mass spectrometer (ThermoStarTM GDS 32, Pfeiffer Vacuum, Germany) was used for the experiment. An FEI QUANTA FEG 200 SEM-EDS electron microscope (Thermo Fisher Scientific, Waltham, MA, USA) was used for the measurements. These experiments involved the analysis of samples of three synthetic samples containing Cl, Br, and I in the presence of $3Na_2O{\cdot}4MoO_3$ solvent. Unfortunately, due to technical reasons, it was not possible to determine the presence of halides in the evolved gas. In the case of $Pb_5(AsO_4)_3Cl_{0.8}(CO_3)_{0.1}$, the thermal analysis showed that up to 976 K, there was no mass loss in the sample, indicative of chlorine evolution. Elemental SEM/EDS analysis of the alloy formed after heating confirmed the presence of Cl (see Supplemental[1] Figure S1a). In the case of $Pb_5(AsO_4)_3Br_{0.8}(CO_3)_{0.1}$, mass loss exceeded that attributable to CO_3 and was below the combined mass of Br and CO_3 in the sample. This result, associated with the presence of Br in the alloy remaining after the experiment (detected by SEM/EDS analysis, see Supplemental[1] Figure S1b), indicates that Br undergoes partial volatilization. In contrast, for $Pb_5(AsO_4)_3I_{0.45}OH_{0.35}(CO_3)_{0.10}$, a significant mass loss occurred in the temperature range from 823 to 976 K. Moreover, SEM/EDS analysis did not show any iodine present in the melt (within the method's detection limit of approximately 0.5 wt% for iodine; see Supplemental[1] Figure S1c). This indicates that all iodine is released from the melted sample at temperatures already lower than the temperature of the calorimetric measurement.

This is the peer-reviewed, final accepted version for American Mineralogist, published by the Mineralogical Society of America.
The published version is subject to change. Cite as Authors (Year) Title. American Mineralogist, in press.
DOI: https://doi.org/10.2138/am-2020-7452. http://www.minsocam.org/

RESULTS

Characteristics of the synthesized products

The synthesis procedure produced white to cream colored homogeneous crystalline powders. The crystals imaged using SEM exhibited hexagonal rod and needle morphologies with sizes ranging from 2 to 5 μm (Sordyl et al. 2020), which is typical for synthetic analogs of minerals of the apatite group. The smallest crystals were observed for $Pb_5(AsO_4)_3I_{0.45}OH_{0.35}(CO_3)_{0.10}$. No other phases were detected by high-resolution synchrotron XRD (Sordyl et al. 2020), SEM, or Raman spectroscopy.

The results of chemical analysis, confirmed by Raman spectroscopy as well as by detailed Rietveld analysis of the structures by Sordyl et al. (2020), yielded the empirical formulas of the synthesized phases shown in Table 1. The molar ratio of Pb/As is theoretically 1.67. The presence of OH groups, apparent on the Raman spectrum, was detected and included in the formula of $Pb_5(AsO_4)_3I$. The presence of CO_3^{2-} was also confirmed by Raman spectroscopy. This result was consistent with the structural analysis presented by Sordyl et al. (2020). The substituion of carbonates is often observed in apatites, resulting from the aqueous synthesis in air (Kwaśniak-Kominek et al. 2017; Lempart et al. 2019). The carbonate content determined by CHNS analysis and estimated by Rietveld structural analysis was 0.16 wt% CO_3^{2-} in $Pb_5(AsO_4)_3OH_{0.86}(CO_3)_{0.07}$, 0.20 wt% in $Pb_5(AsO_4)_3Cl_{0.8}(CO_3)_{0.1}$, and 0.20 wt% in $Pb_5(AsO_4)_3Br_{0.8}(CO_3)_{0.1}$; these values were relatively low. In general, except for $Pb_5(AsO_4)_3I_{0.45}OH_{0.35}(CO_3)_{0.10}$, the amount of substituents was low and did not significantly affect the trends due to halogen and OH substitution in the mimetite structure (Sordyl et al. 2020).

XRD patterns of the synthesis products indicate that they are crystalline analogs of Pb-As apatites (Fig. 1). No other phases were detected with a limit of detection of approximately 0.1 wt% for these phases. Precipitation of other phases was avoided by maintaining the pH at 4.5 during synthesis. Sharp narrow diffraction peaks indicated good crystallinity. The position of the most intense reflection shifted systematically from 29.48°2θ for $Pb_5(AsO_4)_3OH_{0.86}(CO_3)_{0.07}$ to 28.83°2θ for $Pb_5(AsO_4)_3I_{0.45}OH_{0.35}(CO_3)_{0.10}$ due to increasing unit cell size. A detailed structural analysis is presented in Sordyl et al. (2020).

Raman spectra of synthetic halogenated mimetites in the range of 100 to 3600 cm^{-1} are shown in Figure 2. The main bands, the stretching vibration v_1 of the As-O bond, are observed between 806 and 811 cm^{-1}. The scissor vibration bands v_2 of the O-As-O angle are located in the region between 300 and 340 cm^{-1}, and the bending vibration v_4 is observed between 368 and 427 cm^{-1} (Giera et al. 2016). These bands can be further split into two, three, or four bands (Ross 1972). The positions and assignments of the vibrational bands are summarized in Table 2. The positions of all bands shifted slightly toward lower wavelengths with the substitution of the X anion. This shift is systematic, especially for the strongest band (As-O v_1 vibration at approximately 810 cm^{-1}) and its shoulder (v_2 As-O vibration at approximately 760 cm^{-1}, see inset in Figure 2). This is likely not due to a systematic increase in the atomic mass or size of the substituted X anion (Fig. 3). The X ion is located in the hexagonal tunnel of the mimetite structure, separated by Pb cations from the nearest AsO_4 tetrahedra: the X anion mass and size are not expected to significantly affect the As-O bonds, as reflected in the position of the corresponding band on the Raman spectrum (Fig. 3). The cause of the systematic shift observed in the Raman spectra presented in Figure 3 is unclear. The highest frequency bands near 3600 cm^{-1} correspond to the OH stretching modes in the $Pb_5(AsO_4)_3OH_{0.86}(CO_3)_{0.07}$ and $Pb_5(AsO_4)_3I_{0.45}OH_{0.35}(CO_3)_{0.10}$ structures. For $Pb_5(AsO_4)_3OH_{0.86}(CO_3)_{0.07}$, two bands of asymmetric v_3 stretching vibrations are identified at

238 3551.7 cm^{-1} and 3512.1 cm^{-1}, which agrees with previous reports (Giera et al. 2016; Lempart et
239 al. 2019). For $Pb_5(AsO_4)_3I_{0.45}OH_{0.35}(CO_3)_{0.10}$, only one OH stretching vibration is observed at
240 3563.2 cm^{-1} (Fig. 2). The presence of OH groups in $Pb_5(AsO_4)_3I_{0.45}OH_{0.35}(CO_3)_{0.10}$ is due to a
241 partial replacement of I by OH. This finding is consistent with the data of Sordyl et al. (2020).
242 Such substitutions may increase phase stability (Frost et al. 2007). The lack of an extra band in
243 the $Pb_5(AsO_4)_3I_{0.45}OH_{0.35}(CO_3)_{0.10}$ spectrum may be related to the ordering of the anion position
244 in the channel.

245 The presence of CO_3^{2-} ions in the mimetite structures is revealed by the characteristic Raman
246 bands at ~1050 cm^{-1} belonging to the symmetric C-O stretching mode ν_1 (see inset in Figure 2).
247 Giera et al. (2016) identified the same bands for $Pb_5(AsO_4)_3OH$ synthesized under similar
248 conditions. These bands result from carbonate dissolved in aqueous solutions during synthesis in
249 air. The two bands of the carbonate mode v_4 overlapped with the symmetric As-O stretching
250 mode v_1. For $Pb_5(AsO_4)_3OH_{0.86}(CO_3)_{0.07}$, a single band is observed at 1053.3 cm^{-1}, assigned to the
251 v_1 symmetric C-O stretching mode (see Lempart et al. 2019 and literature therein). For
252 $Pb_5(AsO_4)_3Cl_{0.8}(CO_3)_{0.1}$ and $Pb_5(AsO_4)_3Br_{0.8}(CO_3)_{0.1}$, similar v_1 symmetric C-O stretching
253 oscillations are observed at 1040.8 cm^{-1}. The spectrum of $Pb_5(AsO_4)_3I_{0.45}OH_{0.35}(CO_3)_{0.10}$ shows a
254 weak peak at approximately 1059 cm^{-1}, which may indicate a trace amount of carbonate
255 substitution in this structure. For $Pb_5(AsO_4)_3OH_{0.86}(CO_3)_{0.07}$, $Pb_5(AsO_4)_3Cl_{0.8}(CO_3)_{0.1}$, and
256 $Pb_5(AsO_4)_3Br_{0.8}(CO_3)_{0.1}$, the positions of the bands indicate A-type substitution for the X anion,
257 which is consistent with the chemical analysis results shown in Table 1.
258

259 **High-temperature oxide melt calorimetry**

260 The values used in the calculations of $\Delta H°_{f,el}$ are shown in Table 3. The thermodynamic cycles
261 used to calculate the enthalpies of formation of synthetic halogenated mimetites from binary

This is the peer-reviewed, final accepted version for American Mineralogist, published by the Mineralogical Society of America.
The published version is subject to change. Cite as Authors (Year) Title. American Mineralogist, in press.
DOI: https://doi.org/10.2138/am-2020-7452. http://www.minsocam.org/

oxides and elements are presented in Tables 4, 5, 6, and 7. The mean enthalpies of drop solution (ΔH_{DS}) of halogenated mimetites and potassium salts (KCl and KBr) are listed in Supplemental[1] Tables S1–S4 and S5–S6, respectively. Enthalpies of formation from elements $\Delta H°_{f,el}$ for samples containing OH and I were calculated assuming that all the volatiles escaped to the gas phase. In contrast, those for Cl and Br assumed that the halogens remained in the solvent. In all cases, the escape of carbonates into gas was considered. Since the behavior of Br during calorimetry is not clear, a comparative calculation of $\Delta H°_{f,el}$ was performed assuming complete volatilization of Br into the gas phase. The resulting $\Delta H°_{f,el}$ = -2969.7 ± 25.04 (kJ/mol) differs slightly (by only 0.07% relative) from the value calculated assuming that Br remains entirely in the solvent (Table 3). Therefore, although the behavior of KBr in such calorimetric measurements is still awaiting full characterization, in this specific case it does not significantly affected the calculated $\Delta H°_{f,el}$ value for synthetic $Pb_5(AsO_4)_3Br_{0.8}(CO_3)_{0.1}$.

DISCUSSION

Enthalpies of formation of synthetic mimetites

New values of $\Delta H°_{f,el}$ determined experimentally for synthetic arsenate Pb-apatites increased systematically from $Pb_5(AsO_4)_3OH_{0.86}(CO_3)_{0.07}$ (−3030.6 ± 11.5 kJ/mol) through $Pb_5(AsO_4)_3Cl_{0.8}(CO_3)_{0.1}$ (−3026.6 ± 15.8) to $Pb_5(AsO_4)_3Br_{0.8}(CO_3)_{0.1}$ (−2967.6 ± 25.0 kJ/mol). For $Pb_5(AsO_4)_3I_{0.45}OH_{0.35}(CO_3)_{0.10}$, in which iodine is partially substituted by OH groups, $\Delta H°_{f,el}$ was −2993.1 ± 12.2 kJ/mol.

To date, the value of $\Delta H°_{f,el}$ = −2965.9 ± 4.7 kJ/mol for pure synthetic mimetite $Pb_5(AsO_4)_3Cl$ given by Bajda (2010) is the only available experimental result in a series of apatites of lead arsenate. The enthalpy $\Delta H°_{f,el}$ = −3026.6 ± 15.8 kJ/mol determined in this work is 2% lower. However, the difference between the two quantities is so great that it requires a detailed

explanation. The difference is caused by A-type carbonate substitutions in the synthetic mimetite studied herein. Type A carbonate substitutions in hydroxyapatite (HAP) result in a difference of approximately 51.5 kJ/mol in $\Delta H°_{f,el}$ between $Ca_5(PO_4)_3OH$ and $Ca_5(PO_4)_3OH_{0.8}(CO_3)_{0.1}$ (Jebri et al. 2017). Because these are isostructural phases, it is assumed that the carbonate substitutions in mimetite have a similar impact on enthalpy. The chlorine deficiency in our mimetite (0.80 a.p.f.u. Cl) is compensated by the carbonate ion. This deficiency is much smaller for Bajda's (2010) mimetite, in which the chlorine content is 0.976 a.p.f.u. Bajda's mimetite is probably not carbonate-free, as most lead apatites are synthesized from aqueous solutions open to the air (Kwaśniak-Kominek et al. 2015, 2017; Lempart et al. 2019). This is indicated by IR spectra that showed low-intensity bands from carbonates in the 1000-1100 cm^{-1} range (see Figure 2 in Bajda 2010). However, the much lower carbonate content makes the enthalpy value $\Delta H°_{f,el}$ determined by Bajda (2010) less negative by approximately 60.7 kJ/mol.

All synthetic analogs of the mimetite in the present study contain substitutions. The deficiency of Cl and Br is compensated by carbonate ions, and the substitution of OH and carbonate occurs in $Pb_5(AsO_4)_3I_{0.45}OH_{0.35}(CO_3)_{0.10}$. These substitutions were carefully considered when calculating the experimental $\Delta H°_{f,el}$. Thus far, the effect of carbonates on the stability of mimetites expressed by the $\Delta H°_{f,el}$ function has not been studied. The mole contents of CO_3^{2-} are similar for all the tested phases. From the relationships of the results discussed below, it is assumed that the effect of the presence of carbonate ions is small and similar for all phases discussed (but non-negligible). Therefore, the mutual relationships between $\Delta H°_{f,el}$ observed in Figure 4 for other series of calcium and lead apatites are also preserved for the synthetic apatite-like phases investigated here.

Variations in $\Delta H°_{f,el}$ in the apatite supergroup

This is the peer-reviewed, final accepted version for American Mineralogist, published by the Mineralogical Society of America.
The published version is subject to change. Cite as Authors (Year) Title. American Mineralogist, in press.
DOI: https://doi.org/10.2138/am-2020-7452. http://www.minsocam.org/

By making $\Delta H°_{f,el}$ data available for the first time for several analogs of mimetite with different halogenic substitutions, it is possible to show and explain the systematic variation in $\Delta H°_{f,el}$ values within the apatite supergroup. For this purpose, data were compared for all known varieties of calcium and lead apatites containing PO_4 or AsO_4. Using the data given in Table 8, several graphs were plotted showing the variation with respect to some parameters potentially affecting the enthalpic stability or structure of the apatites.

A comparison of the $\Delta H°_{f,el}$ results obtained in this work with the existing data for other apatites containing different anions at the X position (calcium and lead phosphates and arsenates with the apatite structure) is shown in Figure 4a and 4b. The new $\Delta H°_{f,el}$ values vary according to the trends observed for other apatites: the values increased (are less negative) with increasing molar mass, and the effect of substitution of anions at the X position was similar for all these apatites. The only reported value of $\Delta H°_{f,el}$ for $Pb_5(AsO_4)_3Cl_{0.8}(CO_3)_{0.1}$ (Bajda 2010) is at a similar position on the graph as that observed in this study (Fig. 4b).

For all apatites, $\Delta H°_{f,el}$ increases with the ionic radius of X^- (Fig. 5a). This relationship is highly linear and surprisingly similar between the different apatite groups. A similar correlation was noted by Drouet (2015), who only analyzed the phosphate Ca-apatite group. Drouet (2015, 2019) also found no correlation of $\Delta H°_{f,el}$ with the size of the Me^{2+} cation in apatite. This implies that the similarities observed in the patterns of variability of $\Delta H°_{f,el}$ from the X^- radius for different apatites are very significant. It can be contended that the radius of X^- is a predominant factor contributing to their thermodynamic stability for all apatites. In all cases, the position of OH-apatites deviates from the line determined by a series of halides. Therefore, all correlation lines were plotted only on the basis of data for halogenated apatites. The value of $\Delta H°_{f,el}$ for OH-apatites corresponded to an ionic radius of larger than 1.37 Å used for the OH group. This implies that the effective radius of OH affecting the properties of HAP is greater. The main

feature differentiating the OH ion from halide anions is its anisotropy: the charge of the OH ion is not evenly distributed in space due to the presence of the H^+ proton. The presence of such an anion in the hexagonal tunnel of the apatite crystalline structure imposes a higher energy penalty; thus, the enthalpy of formation $\Delta H°_{f,el}$ is higher (more endothermic). There also exist other modifications, e.g., the presence of H^+ on the OH^- group can lead to hydrogen bonding effects within apatite channels, probably causing a stabilizing effect. Additionally, the OH^- ions in the X-position ions in the channels within the apatite structure do not occupy the same positions in the *z* value along the *c*-axis. The larger the X-site anion is, the more separated it is from the mirror plane of the triangular cationic II sites. Therefore, in all cases, the data for OH-apatites plot above the line are determined by a series of halogenated apatites. Because of the mixed nature of $Pb_5(AsO_4)_3I_{0.45}OH_{0.35}(CO_3)_{0.10}$, the value of $\Delta H°_{f,el}$ for this phase is closer to $\Delta H°_{f,el}$ of $Pb_5(AsO_4)_3OH_{0.86}(CO_3)_{0.07}$ and plotted below this line on the graph. The value previously determined by Bajda (2010) for pure synthetic mimetite $Pb_5(AsO_4)_3Cl$ is also included.

An important parameter linking $\Delta H°_{f,el}$ in an isomorphic series is Pauling's electronegativity of X. In this approximation, an oxygen electronegativity of $\chi_O = 3.51$ was assumed for the OH group. The plot in Figure 5b of electronegativity versus $\Delta H°_{f,el}$ for apatites yields a linear correlation and similar variation for all the apatite groups discussed. The position of $Pb_5(AsO_4)_3I_{0.45}OH_{0.35}(CO_3)_{0.10}$ slightly below and $Pb_5(AsO_4)_3OH_{0.86}(CO_3)_{0.07}$ slightly above the line drawn by the other phases of the studied series is observed.

Drouet (2015) introduced the ionic character of the Me-X bond denoted as I′. It is defined from the electronegativity values of Me and X as (Equation 1):

$$I' = 0.46|\chi_{Me} - \chi_X| + 0.035(\chi_{Me} - \chi_X)^2 \quad (1)$$

where χ_{Me} and χ_X are the electronegativities of the metal (Ca or Pb) and halide, respectively. The correlation of I′ with $\Delta H°_{f,el}$ shown in Figure 5c is analogous to the correlation with the

358 electronegativity of X. Although such a Me-X bond does not exist, the course of both presented
359 relationships unequivocally showed that, as observed by Drouet (2015), the effect of halide
360 electronegativity on the thermodynamic stability of calcium apatites is the same for all the
361 discussed groups of apatites, regardless of Me^{2+} cation or PO_4^{3-} and AsO_4^{3-} anion. A similar
362 effect of the difference in electronegativity between Me and X on the stability of apatite might
363 also be observed. Despite the simplifying assumption for the electronegativity of OH, the plot
364 location of OH-apatites hardly deviates from the trend line corresponding to halides for
365 phosphate apatites of the calcium and lead series. The plot location of
366 $Pb_5(AsO_4)_3I_{0.45}OH_{0.35}(CO_3)_{0.10}$, for which iodine electronegativity was used, is below the line,
367 again indicating the influence of OH substitution for I. This is also consistent with the values of
368 $\Delta H°_{f,el}$ determined in this study for correct mimetites and reflects the trends observed for all
369 apatites.

370 A surprisingly linear correlation was obtained by plotting the dependence on the first
371 ionization energy of the element X versus $\Delta H°_{f,el}$ of selected apatites (Fig. 5d). It was anticipated
372 that this value may indirectly reflect the ionic affinity between the X^- ion and the apatite
373 structure. Again, the value for oxygen is used as a proxy for OH, and the OH-apatites are not
374 included in the regression lines determined by halides.

375 Cruz et al. (2005) noted a very good linear relationship between the enthalpy of the formation
376 of calcium P-apatites and that of the formation of calcium halides (or oxides) (i.e., MeX_2
377 compounds). An extended comparison is shown in Figure 5e. The same linear relationship is
378 observed for all apatites. The projection of points for HAP deviates slightly from the trends
379 determined by halides: for both series of lead apatites, it is slightly (within the error limits) above
380 the line determined by halides. The position of $Pb_5(AsO_4)_3I_{0.45}OH_{0.35}(CO_3)_{0.10}$ was slightly below
381 the trend line, as expected. Thus, a positive correlation of $\Delta H°_{f,el}$ of apatites with $\Delta H°_{f,el}$ of MeX_2

This is the peer-reviewed, final accepted version for American Mineralogist, published by the Mineralogical Society of America.
The published version is subject to change. Cite as Authors (Year) Title. American Mineralogist, in press.
DOI: https://doi.org/10.2138/am-2020-7452. http://www.minsocam.org/

exists, indicating that the thermodynamic stability in the isomorphic series of anion X-substituted apatites is closely linked to that of the corresponding MeX_2 compounds. This relationship is identical for all apatites.

Some generalizations can be made about $Pb_5(AsO_4)_3I_{0.45}OH_{0.35}(CO_3)_{0.10}$. $Pb_5(AsO_4)_3I_{0.45}OH_{0.35}(CO_3)_{0.10,}$ obtained as described here, is an intermediate phase of the $Pb_5(AsO_4)_3I$ – $Pb_5(AsO_4)_3OH$ series. This indicates the likelihood of a continuous series of isomorphic substitutions of OH for I within the mimetites; however, this series was not the focus here. The results indicate that OH substitutions in $Pb_5(AsO_4)_3I$ increase $\Delta H°_{f,el}$ ($\Delta H°_{f,el}$ becomes more endothermic). Figure 5 shows that the value determined in this work for $Pb_5(AsO_4)_3I_{0.45}OH_{0.35}(CO_3)_{0.10}$ is close to the intermediate value between $\Delta H°_{f,el}$ for $Pb_5(AsO_4)_3OH_{0.86}(CO_3)_{0.07}$ and $\Delta H°_{f,el}$ expected for pure $Pb_5(AsO_4)_3I$ based on the regression line. It is, however, plotted closer to the position expected for pure $Pb_5(AsO_4)_3I$ than the intermediate position between I-OH. This indicates that the substitution of OH in $Pb_5(AsO_4)_3I$ has a small effect on the change in its thermodynamic properties and that $Pb_5(AsO_4)_3I$ dominates. The pure $Pb_5(AsO_4)_3I$ is probably enthalpically the least stable of the entire subgroup discussed here (it has the most positive $\Delta H°_{f,el}$). These relationships require confirmation through studies of the $Pb_5(AsO_4)_3I$ – $Pb_5(AsO_4)_3OH$ series and thermodynamic characterization of the intermediate phases.

Predictions of $\Delta H°_{f,el}$ for pure endmembers

Analysis of Figure 5 shows that for all the existing data for the analyzed apatites, the enthalpy of formation $\Delta H°_{f,el}$ changes linearly with (1) electronegativity, (2) the ionic character of the bond Me-X, (3) the first ionization energy of the element X, and (4) the enthalpy of the formation of MeX_2. An extrapolation of the trend lines presented in Figures 5 a-e was used to estimate the

This is the peer-reviewed, final accepted version for American Mineralogist, published by the Mineralogical Society of America.
The published version is subject to change. Cite as Authors (Year) Title. American Mineralogist, in press.
DOI: https://doi.org/10.2138/am-2020-7452. http://www.minsocam.org/

406 value of $\Delta H°_{f,el}$ predicted for $Pb_5(AsO_4)_3F$. The obtained values are −3215.4, −3087.4, −3090.1,
407 −3252.7, and −3076.1 kJ/mol. The arithmetic mean of the $\Delta H°_{f,el}$ values thus estimated for
408 $Pb_5(AsO_4)_3F$ is −3144.3 ± 66.5 (error represents two standard errors $2\sigma_M$ of the mean). The value
409 is currently the only existing data of $\Delta H°_{f,el}$ for $Pb_5(AsO_4)_3F$ and can be used as an approximation
410 in other calculations until it is determined experimentally.

411 Another tool to estimate $\Delta H°_{f,el}$ is the use of thermochemical cycles based on lattice energies
412 (U_{POT}) proposed by Flora et al. (2004). Unfortunately, because of the lack of data for the enthalpy
413 of formation and the enthalpy of hydration for gaseous AsO_4^{3-} ($\Delta H°_{f,\ AsO43-,g}$ and $\Delta H°_{hydration,\ AsO43-,g,}$ respectively), the experimental values of $\Delta H°_{f,el}$ or U_{POT} cannot be determined directly.
415 Therefore, for As-apatites, thermochemical cycles proposed by Flora et al. (2004) are not relevant
416 here. However, the Glasser-Jenkins Equation 3 (Glasser and Jenkins 2000) supports the
417 calculation of U_{POT} values based on the measured or calculated volume of a unit cell:

418 $$U_{POT}\ (\frac{kJ}{mol}) = 26680 \times {V_m}^{1/3} \quad (3)$$

419 where U_{POT} is the estimated lattice energy in kJ/mol and V_m is the measured volume of a crystal
420 unit cell in nm^3. Flora et al. (2004) examined the difference between the U_{POT} obtained using
421 Equation (3) and the experimental U_{POT} calculated using appropriate thermochemical cycles. The
422 error for lead phosphate apatites (pyromorphites, most similar to mimetites) was relatively large
423 at 8% (Flora et al. 2004). However, an attempt was made to perform such calculations because
424 the lattice enthalpy is directly related to the enthalpy of apatite formation, and we have lattice
425 volumes V_m obtained for these mimetites from high-resolution synchrotron PXRD data (Sordyl et
426 al. 2020). This estimation may be useful, e.g., for the prediction of $\Delta H°_{f,\ el}$ $Pb_5(AsO_4)_3F$, for
427 which calorimetric determination is not currently feasible for technical reasons. The results are
428 shown in Table 9 and Figure 6b. As with the other relationships discussed above, the correlations

observed in the halogen series are linear. The line is determined by three points: $Pb_5(AsO_4)_3OH_{0.86}(CO_3)_{0.07}$, $Pb_5(AsO_4)_3Cl_{0.8}(CO_3)_{0.1}$, and $Pb_5(AsO_4)_3Br_{0.8}(CO_3)_{0.1}$. Similar to the plots in Figure 5, the value determined for $Pb_5(AsO_4)_3I_{0.45}OH_{0.35}(CO_3)_{0.10}$ plots slightly downward due to the substitution of I with OH.

Based on the linear regression shown in Figure 6a, extrapolation was performed, and the estimated $Pb_5(AsO_4)_3F$ value was $\Delta H°_{f,\,el} = -3152 \pm 267$ kJ/mol. This predicted value differs only slightly from the value of -3144 ± 67 kJ/mol estimated above from the relationship in Figure 5. The agreement of the results obtained from the independent predictions strongly strengthens the confidence in the results obtained. However, experimental confirmation is required in the future. Additionally, similar correlations are observed using the U_{POT} calculated by Flora et al. (2004) and selected $\Delta H°_{f,el}$ for Pb and Ca P-apatites with different halogen substituents (see Supplemental[1] Figure S2 and Supplemental[1] Table S9). On the basis of these correlations, an attempt was made to extrapolate $\Delta H°_{f,\,el}$ for $Pb_5(PO_4)_3I$ and $Ca_5(PO_4)_3I$, resulting in $\Delta H°_{f,\,el} = -4021 \pm 148$ and $\Delta H°_{f,\,el} = -6423 \pm 76$ kJ/mol, respectively.

The value presented here for $Ca_5(PO_4)_3I$ differed from $\Delta H°_{f,\,el} = -6475 \pm 60$ kJ/mol obtained by Cruz et al. (2005) and $\Delta H°_{f,\,el} = -6450 \pm 200$ kJ/mol from the SSA model obtained by Glasser (2019) by only approximately 0.8% and 0.4%, respectively.

The $\Delta H°_{f,el}$ for the studied phases can be compared with the predictions. The estimation or prediction of thermodynamic data for apatites has attracted the interest of many scientists (see, e.g., Flora et al. 2004; Iglesia 2009; Drouet 2015; Glasser 2019 and the literature cited therein). The majority of the work has been conducted on phosphate apatites (Drouet 2015). A recent paper by Glasser (2019) describes the application of the so-called simple salt approximation (SSA) model of Yoder and Flora (2005) to simplify calculations of $\Delta H°_{f,el}$ for both phosphate and

arsenate apatites, including mimetite $Pb_5(AsO_4)_3Cl$. The calculation is based on the application of Equation 2 (after Glasser 2019, modified):

$$\Delta H^\circ_{f,el\ of\ apatite} = 1.5 \times \Delta H^\circ_{f,el}\,(As_2O_5) + 0.5 \times \Delta H^\circ_{f,el}\,(PbX_2) \quad (2)$$

where X = F, OH, Cl, Br, or I. Our experimental results and calculations using the SSA model differed from 3.3% to 7.8% (Table 9). The discrepancies are evident in Figure 6b: the slope of the line related to the values determined by both methods is far from 1. Although our synthetic analogs of mimetite contain substitutions, this finding is in line with Glasser's (2019) opinion that using the SSA model to evaluate the thermochemical data for arsenic apatites is not recommended as it is affected by large errors.

IMPLICATIONS

The determination and estimation of $\Delta H^\circ_{f,el}$ for a wide group of synthetic lead arsenate apatite-like phases isostructural with mimetite with different anion substitutions in the X position (X = OH, Cl, Br, and I) have allowed us for the first time to compile and compare values between Ca-, Pb-, P-, and As-apatites. This uncovered many systematic relationships hitherto unknown, indicating that the thermodynamic enthalpic stability is largely influenced by chemical factors (e.g., differences in electronegativities of elements, ionization energy, or ionic characteristics of the bonds) and probably to a lesser extent by physical and geometric parameters in the crystal structure that are related to the mass and size of the X anion. A major implication of such a comparison of the data is the conjecture that the observed relationships are universal for the entire apatite supergroup and can be used to predict the expected values of $\Delta H^\circ_{f,el}$ for phases that have not been studied experimentally. The presented explanation of the regular variability in $\Delta H^\circ_{f,el}$

within the Ca- and Pb-apatites contributes significantly to the understanding of apatites as a whole mineral supergroup.

To date, synthetic $Pb_5(VO_4)_3I$ and $Ca_5(PO_4)_3(I,OH)$ have been proposed as potential hosts for I-129 (Hassan and Ryu 2019; Guo et al. 2020), but the easy-to-synthesize $Pb_5(AsO_4)_3I_{0.45}OH_{0.35}(CO_3)_{0.10}$ discussed here is also a promising phase belonging to the apatite supergroup. It remains unclear how these apatite waste forms will be deposited in a repository and how they will behave in the presence of infiltrating water. Because of the long half-life of I-129, it is critical to predict the long-term chemical stability of iodine waste forms. To enable such predictions, computer simulations of the reactions, and modeling of the processes involved, it is necessary to obtain basic thermodynamic data. The direct experimental determination of thermodynamic parameters such as $\Delta H°_{f,el}$ and solubility constants K_{sp} is challenging. The presented experimental methods coupled with theoretical calculations and predictions bring us closer to this goal.

The results of this work also allow us to comment on two different methods for determining $\Delta H°_{f,el}$. Although faster and more direct, calorimetric measurement requires high-quality analytical equipment and high precision. Because of technical and equipment limitations, it is sometimes difficult or impossible to perform such measurements for certain substances (e.g., $Pb_5(AsO_4)_3F$). Determination of the enthalpy of formation can also be accomplished by dissolution experiments in aqueous solutions and by determining the variation of the solubility constant K_{sp} with T. This technique also has limitations for many substances. It is used for substances showing measurable solubility in aqueous solutions. Although it is time-consuming, the precision of the determinations does not differ from that of calorimetric measurements. Therefore, in further studies, an attempt will be made to verify the calorimetric data $\Delta H°_{f,el}$ by direct experimental determination of K_{sp} at different temperatures for $Pb_5(AsO_4)_3X$ (where X=F,

499 OH, Cl, Br, I). For such, calorimetric measurements are difficult, and the only data available are
500 values estimated from the prediction based on the correlation of values already determined.
501
502 **Acknowledgments**: We greatly appreciate the comments of AM Associate Editor Charles A.
503 Geiger and the four anonymous reviewers, which have helped us to improve the manuscript. I am
504 grateful for the brainstorming session with Małgorzata Lempart-Drozd, which helped to
505 definitely improve the quality of the discussion of the results obtained. Many thanks to my friend
506 Grzegorz Rzepa for the time we spent together on the SEM/EDS analyses, which proved to be
507 revealing. Financial support for the research was provided to B.P. by the Polish National Science
508 Center (NCN) [Grant No. 2017/27/N/ST10/00776]. The calorimetry portion of this work was
509 funded by the Chemical Sciences, Geosciences and Biosciences Division, Office of Basic Energy
510 Sciences, Office of Science, U.S. Department of Energy [Grant No. DE-FG02–07ER15880].
511

512 **REFERENCES**

513 Bajda, T. (2010) Solubility of mimetite $Pb_5(AsO_4)_3Cl$ at 5–55 °C. Environmental Chemistry, 7,
514 268–278.
515 Baker, W.E. (1966) An X-ray diffraction study of synthetic members of the pyromorphite series.
516 American Mineralogist, 51, 1712–1721.
517 Cao, S., Zhang, Z.L., Dai, L.Q., Zhu, Y.N., Zhu, Z.Q., Tan, L.L., and Wei, C.C. (2014) The
518 calculation of physicochemical parameters in the mimetite dissolving process. Advanced Material
519 Research, 860, 1035–1039.
520 Chappell, M.A., and Scheckel, K.G. (2007) Pyromorphite formation and stability after quick lime
521 neutralisation in the presence of soil and clay sorbents. Environmental Chemistry, 4, 109–113.

Cohen, B.L. (1977) High-level radioactive waste from light-water reactors. Reviews of Modern Physics, 49, 1.

Comba, P.G. (1987) Removal of arsenic from process and wastewater solutions, 43 p. M.Sc. thesis, Montana College of Mineral Science and Technology, Butte.

Conca, J., Wright, J., and Triay, I. (2000) Pims: a simple technology for clean-up of heavy metals and radionuclides throughout the world. In T.E. Baca and T. Florkowski, Eds., The environmental challenges of nuclear disarmament, p. 223-236. Springer, Dordrecht.

Cruz, F.J.A.L., da Piedade, M.E.M., and Calado, J.C.G. (2005) Standard molar enthalpies of formation of hydroxy-, chlor-, and bromapatite. Journal of Chemical Thermodynamics, 37, 1061–1070.

Dean, J.A., Ed. (1999) Lange's handbook of chemistry, 15th ed., McGrow-Hill, New York.

Dinsdale, A. (1991) SGTE data for pure elements. Calphad-Computer Coupling of Phase Diagrams and Thermochemistry, 15, 317–425.

Drouet, C. (2015) A comprehensive guide to experimental and predicted thermodynamic properties of phosphate apatite minerals in view of applicative purposes. Journal of Chemical Thermodynamics, 81, 143–159.

Drouet, C. (2019) Applied predictive thermodynamics (ThermAP). Part 2. Apatites containing Ni^{2+}, Co^{2+}, Mn^{2+}, or Fe^{2+} ions. The Journal of Chemical Thermodynamics, 136, 182–189.

Fleet, M. E., and Liu, X. (2007) Coupled substitution of type A and B carbonate in sodium-bearing apatite. Biomaterials, 28, 916–926.

Flis, J., Manecki, M., and Bajda, T. (2011) Solubility of pyromorphite $Pb_5(PO_4)_3Cl$–mimetite $Pb_5(AsO_4)_3Cl$ solid solution series. Geochimica et Cosmochimica Acta, 75, 1858–1868.

Flora, N.J., Yoder, C.H., and Jenkins, H.D.B. (2004) Lattice energies of apatites and the estimation of $\Delta H_f°(PO_4^{3-}, g)$. Inorganic Chemistry, 43, 2340–2345.

546 Forray, F.L., Smith, A.M.L., Navrotsky, A., Wright, K., Hudson-Edwards, A., and Dubbin,
547 W.E. (2014) Synthesis, characterization and thermochemistry of synthetic Pb-As, Pb-Cu and Pb-
548 Zn jarosites. Geochimica et Cosmochimica Acta, 127, 107–119.
549 Frost, R.L., Bouzaid, J.M., and Palmer, S. (2007) The structure of mimetite, arsenian
550 pyromorphite and hedyphane–a Raman spectroscopic study. Polyhedron, 26, 2964–2970.
551 Giera, A., Manecki, M., Bajda, T., Rakovan, J., Kwaśniak-Kominek, M., and Marchlewski, T.
552 (2016) Arsenate substitution in lead hydroxyl apatites: a Raman spectroscopic study.
553 Spectrochimica Acta Part A: Molecular and Biomolecular Spectroscopy, 152, 370–377.
554 Glasser, L., and Jenkins, H.D.B. (2000) Lattice energies and unit cell volumes of complex ionic
555 solids. Journal of the American Chemical Society, 122, 632–638.
556 Glasser, L. (2019) Apatite thermochemistry: the simple salt approximation. Inorganic chemistry,
557 58, 13457–13463.
558 Guo, X., Wang, Y., Yao, T., Mohanty, C., Lian, J., and Frankel, G.S. (2020) Corrosion
559 interactions between stainless steel and lead vanado-iodoapatite nuclear waste form part I. Nature
560 Partner Journals Materials Degradation, 4, 1–12.
561 Hassan, M.U., and Ryu, H.J. (2019) Cold sintering and durability of iodate-substituted calcium
562 hydroxyapatite (IO-HAp) for the immobilization of radioiodine. Journal of Nuclear Materials,
563 514, 84–89.
564 Hughes, J.M., and Rakovan, J.F. (2015) Structurally robust, chemically diverse: apatite and
565 apatite supergroup minerals. Elements, 11, 165–170.
566 Iglesia, A.L. (2009) Estimating the thermodynamic properties of phosphate minerals at high and
567 low temperature from the sum of constituent units. Estudios Geológicos, 65, 109–119.

Jebri, S., Khattech, I., and Jemal, M. (2017) Standard enthalpy, entropy and Gibbs free energy of formation of «A» type carbonate phosphocalcium hydroxyapatites. The Journal of Chemical Thermodynamics, 106, 84–94.

Jie, K., Zhou, Y., Li, E., Li, Z., Zhao, R., and Huang, F. (2017) Reversible iodine capture by nonporous pillar[6]arene crystals. Journal of the American Chemical Society, 139, 15320–15323.

Karna, R., Noerpel, M., Luxton, T., and Scheckel, K. (2018) Point of zero charge: role in pyromorphite formation and bioaccessibility of lead and arsenic in phosphate-amended soils. Soil Systems, 2, 22.

Kwaśniak-Kominek, M., Matusik, J., Bajda, T., Manecki, M., Rakovan, J., Marchlewski, T., and Szala, B. (2015) Fourier transform infrared spectroscopic study of hydroxylpyromorphite $Pb_{10}(PO_4)_6OH_2$–hydroxylmimetite $Pb_{10}(AsO_4)_6(OH)_2$ solid solution series. Polyhedron, 99, 103–111.

Kwaśniak-Kominek, M., Manecki, M., Matusik, J., and Lempart, M. (2017) Carbonate substitution in lead hydroxyapatite $Pb_5(PO_4)_3OH$. Journal of Molecular Structure, 1147, 594–602.

Laperche, V., Logan, T.J., Gaddam, P., and Traina, S.J. (1997) Effect of apatite amendments on plant uptake of lead from contaminated soil. Environmental Science and Technology, 31, 2745–2753.

Lei, P., Yao, T., Gong, B., Zhu, W., Ran, G., and Lian, J. (2020) Spark plasma sintering-densified vanadinite apatite-based chlorine waste forms with high thermal stability and chlorine confinement. Journal of Nuclear Materials, 528, 151857–151864.

Lempart, M., Manecki, M., Kwaśniak-Kominek, M., Matusik, J., and Bajda, T. (2019) Accommodation of the carbonate ion in lead hydroxyl arsenate (hydroxylmimetite) $Pb_5(AsO_4)_3OH$. Polyhedron, 161, 330–336.

Liu, H.L., Zhu, Y.N., and Yu, H.X. (2009) Solubility and stability of lead arsenates at 25 °C. Journal of Environmental Science and Health Part A-Environmental Science and Engineering and Toxic and Hazardous Substance Control, 44, 1465–1475.

Ma, S., Islam, S.M., Shim, Y., Gu, Q., Wang, P., Li, H., Sun G., Yang X., and Kanatzidis, M.G. (2014) Highly efficient iodine capture by layered double hydroxides intercalated with polysulfides. Chemistry of Materials, 26, 7114–7123.

Majzlan, J., Navrotsky, A., and Neil, J.M. (2002) Energetics of anhydrite, barite, celestine, and anglesite: A high-temperature and differential scanning calorimetry study. Geochimica et Cosmochimica Acta, 66, 1839–1850.

Manecki M., Bogucka A., Bajda T., and Borkiewicz O. (2006) Decrease of Pb bioavailability in solis by addition of phosphate ions. Environmental Chemistry Letters, 3, 178–181.

Manecki, M., Bajda, T., Wegner, M., and Borkiewicz, O. (2009) Immobilization of Pb(II) by crystallization of pyromorphite on galena in the presence of phosphate fertilizers. Geologia / Akademia Górniczo-Hutnicza im. Stanisława Staszica w Krakowie - Geology, Geophysics and Environment, 35, 263–269 (in Polish).

Manecki, M. (2020) Lead in water and soil: speciation, toxicity, and treatment technologies. In P.A. Maurice, Ed., Encyclopedia of Water: Science, Technology, and Society, p. 1713-1727. Wiley and Sons, U.K.

Marciniak, H., Diduszko, R., and Kozak, M. (2006) XRAYAN - Program do rentgenowskiej analizy fazowej, KOMA, Warsaw (in Polish).

Merker, L., and Wondratschek, H. (1959) Bleiverbindungen mit apatitstruktur, insbesondere blei–jod-und blei–brom-apatite. Zeitschrift für Anorganische und Allgemeine Chemie, 300, 41–50 (in German).

614 Navrotsky, A. (1977) Progress and new directions in high-temperature calorimetry revisited.
615 Physics and Chemistry of Minerals, 2, 89–104.
616 Navrotsky, A. (1997) Progress and new directions in high temperature calorimetry revisited.
617 Physics and Chemistry of Minerals, 24, 222–241.
618 Navrotsky, A. (2014) Progress and new directions in calorimetry: A 2014 Perspective. Journal of
619 American Ceramic Society, 97, 3349–3359.
620 Nordstrom, D.K., Majzlan, J., and Königsberger, E. (2014) Thermodynamic properties for
621 arsenic minerals and aqueous species. Reviews in Mineralogy and Geochemistry, 79, 217–255.
622 Nriagu, J.O. (1974) Lead orthophosphates - Formation and stability in the environment.
623 Geochimica et Cosmochimica Acta, 38, 887–898.Pauling, L. (1988) General chemistry, 183 p.
624 Courier Corporation, New York.
625 Rakovan, J.F., and Pasteris, J.D. (2015) A technological gem: materials, medical, and
626 environmental mineralogy of apatite. Elements, 11, 195–200.
627 Rigali, M.J., Brady, P.V., and Moore, R.C. (2016) Radionuclide removal by apatite. American
628 Mineralogist, 101, 2611–2619.
629 Robie, R.A., and Hemingway, B.S. (1995) Thermodynamic properties of minerals and related
630 substances at 298.15 K and 1 bar (10^5 Pascals) pressure and at higher temperatures, 2131, 461 p.
631 US Government Printing Office, Washington.
632 Ross, S.D. (1972) Inorganic infrared and Raman spectra, 329 p. McGrow-Hill, New York.
633 Ruby, M.V., Davis, A., and Nicholson, A. (1994) In situ formation of lead phosphates in soils as
634 a method to immobilize lead. Environmental Sciences and Technology, 28, 646–654.
635 Sava, D.F., Garino, T.J., and Nenoff, T.M. (2012) Iodine confinement into metal–organic
636 frameworks (MOFs): low-temperature sintering glasses to form novel glass composite material
637 (GCM) alternative waste forms. Industrial and Engineering Chemistry Research, 51, 614–620.

638 Shannon, R.T., and Prewitt, C.T. (1969) Effective ionic radii in oxides and fluorides. Acta
639 Crystallographica Section B-Structural Science, 25, 925–946.
640 Shvareva, T.Y., Fein, J.B., and Navrotsky, A. (2012) Thermodynamic properties of uranyl
641 minerals. Constraints from calorimetry and solubility measurements. Industrial and Engineering
642 Chemistry Research, 51, 607–613.
643 Sordyl, J., Puzio, B., Manecki, M., Borkiewicz, O., Topolska, J., and Zelek-Pogudz, S. (2020)
644 Structural assessment of fluorine, chlorine, bromine, iodine, and hydroxide substitutions in lead
645 arsenate apatites (mimetites)–$Pb_5(AsO_4)_3X$. Minerals, 10, 494.
646 Stull, D.R., and Prophet, H. (1971) JANAF thermochemical tables, 2nd ed., 1141 p. US National
647 Bureau of Standards NSRDS-NBS-37, Washington, DC.
648 Topolska, J., Latowski, D., Kaschabek, S., Manecki, M., Merkel, B.J., and Rakovan, J. (2014) Pb
649 remobilization by bacterially mediated dissolution of pyromorphite $Pb_5(PO_4)_3Cl$ in presence of
650 phosphate-solubilizing Pseudomonas putida. Environmental Science and Pollution Research, 21,
651 1079–1089.
652 Twidwell, L.G., Plessas, K.O., Comba, P.G., and Dahnke, D.R. (1994) Removal of arsenic from
653 wastewaters and stabilization of arsenic bearing waste solids: summary of experimental studies.
654 Journal of Hazardous Materials, 36, 69–80.
655 Yoder, C.H., and Flora, N.J. (2005) Geochemical applications of the simple salt approximation to
656 the lattice energies of complex materials. American Mineralogist, 90, 488–496.
657 Zhang, L., Dzik, E.A., Sigmon, G.E., Szymanowski, J.E., Navrotsky, A., and Burns, P.C. (2018)
658 Experimental thermochemistry of neptunium oxides: Np_2O_5 and NpO_2. Journal of Nuclear
659 Materials, 501, 398–403.
660

661 **Endnote:**

This is the peer-reviewed, final accepted version for American Mineralogist, published by the Mineralogical Society of America.
The published version is subject to change. Cite as Authors (Year) Title. American Mineralogist, in press.
DOI: https://doi.org/10.2138/am-2020-7452. http://www.minsocam.org/

662 [1]Deposit item AM-……., Supplemental Material and Figures. Deposit items are free to all
663 readers and found on the MSA website, via the specific issue's Table of Contents.

664

665 **List of Figures**

666 **Figure 1.** XRD patterns of halogenated mimetites. The regular shift of the peak position toward
667 lower 2θ values is observed from $Pb_5(AsO_4)_3OH_{0.86}(CO_3)_{0.07}$ to $Pb_5(AsO_4)_3I_{0.45}OH_{0.35}(CO_3)_{0.1}$.

668 **Figure 2.** Raman spectra of synthetic halogenated analogs of mimetite.

669 **Figure 3.** The position of the two most intense As-O bands for $Pb_5(AsO_4)_3X$ (where X=OH, Cl,
670 Br, I), the scissor vibration bands v_2 of the O-As-O angle (triangles) and the asymmetric
671 stretching vibrations v_3 (diamonds) in the Raman spectrum are systematically determined (**a**), but
672 this is not reflected by the relationship with the atomic radius of anion X (**b**) or with the atomic
673 mass of anion X (**c**).

674 **Figure 4.** Plot of the existing data of $\Delta H°_{f,el}$ for (**a**) $Ca_5(PO_4)_3X$ (squares) and $Ca_5(AsO_4)_3X$
675 (triangles) and (**b**) $Pb_5(PO_4)_3X$ (circles) and $Pb_5(AsO_4)_3X$ (diamonds), with different halogen
676 substitutions (where X=F, OH, Cl, Br, I) versus their molar masses. The position of the only
677 existing literature data for $Pb_5(AsO_4)_3Cl$ (rectangle) determined by Bajda (2010) is also
678 presented.

679 **Figure 5.** Effects of various parameters, such as the ionic radius of X^- (**a**), χ_x electronegativity of
680 X (**b**), I' ionic character of Me – X bond (Me=Ca, Pb) (**c**), E^+ ionization energy of X (**d**), and
681 $\Delta H°_{f,el}$ of MeX_2 binary compounds (**e**), on the thermodynamics of $Ca_5(PO_4)_3X$ (squares),
682 $Ca_5(AsO_4)_3X$ (triangles), $Pb_5(PO_4)_3X$ (circles) and $Pb_5(AsO_4)_3X$ (diamonds) with different
683 halogenic substitutions (where X=F, OH, Cl, Br, I). $\Delta H°_{f,el}$ marked with an empty marker were
684 not included in the trend. The pattern-filled markers for $Pb_5(AsO_4)_3F$ illustrate the estimated

This is the peer-reviewed, final accepted version for American Mineralogist, published by the Mineralogical Society of America.
The published version is subject to change. Cite as Authors (Year) Title. American Mineralogist, in press.
DOI: https://doi.org/10.2138/am-2020-7452. http://www.minsocam.org/

685 $\Delta H°_{f,el}$ values from the extrapolation of the trend lines. The position of the only existing literature
686 data for $Pb_5(AsO_4)_3Cl$ (rectangle) determined by Bajda (2010) is also presented.

687 **Figure 6.** Plots of $\Delta H°_{f,el}$ of mimetites (diamonds) determined by calorimetry (this work) versus
688 $\Delta H°_{f,el}$ calculated using the SSA model by Glasser (**a**) and calculated lattice energies (U_{POT}) (**b**).
689 The $\Delta H°_{f,el}$ of $Pb_5(AsO_4)_3F$ (triangle) was extrapolated from the presented trend line. The $\Delta H°_{f,el}$
690 of $Pb_5(AsO_4)_3I_{0.45}OH_{0.35}(CO_3)_{0.1}$ (empty diamond) was not included in the trend line.
691
692
693
694
695
696
697
698
699
700
701
702
703
704
705
706
707
708

This is the peer-reviewed, final accepted version for American Mineralogist, published by the Mineralogical Society of America.
The published version is subject to change. Cite as Authors (Year) Title. American Mineralogist, in press.
DOI: https://doi.org/10.2138/am-2020-7452. http://www.minsocam.org/

709

710

711 **Tables**

712 Table 1. Chemical composition of synthetic analogs of mimetite.

Ideal Chemical Formula	Empirical Chemical Formula
$Pb_5(AsO_4)_3Cl$	$Pb_{5.00\pm0.02}(AsO_4)_{3.00\pm0.04}Cl_{0.80\pm0.05}(CO_3)_{0.10\pm0.02}$
$Pb_5(AsO_4)_3Br$	$Pb_{5.00\pm0.02}(AsO_4)_{3.00\pm0.05}Br_{0.80\pm0.03}(CO_3)_{0.10\pm0.02}$
$Pb_5(AsO_4)_3I$	$Pb_{5.00\pm0.03}(AsO_4)_{3.00\pm0.02}I_{0.45\pm0.02}\ OH_{0.35}(CO_3)_{0.10\pm0.02}$
$Pb_5(AsO_4)_3OH$	$Pb_{5.00\pm0.02}\ (AsO_4)_{3.00\pm0.03}OH_{0.86}(CO_3)_{0.07\pm0.02}$

713

714

715

716

717

718

719

720

721

722

723

724

725

726

This is the peer-reviewed, final accepted version for American Mineralogist, published by the Mineralogical Society of America.
The published version is subject to change. Cite as Authors (Year) Title. American Mineralogist, in press.
DOI: https://doi.org/10.2138/am-2020-7452. http://www.minsocam.org/

727

728

729 Table 2. List of Raman bands for $Pb_5(AsO_4)_3X$ (where X=Cl, Br, I, OH) and selected parameters

730 for plotting Figure 3.

Bands (cm^{-1})/species (X)	Cl	Br	(I,OH)	OH
v_1	810.7	810.3	807.4	806.6
v_2	336.0	332.0	332.0	340.0
v_3	766.2	757.7	748.0	777.1
v_4	370.0	371.0	372.0	368.0
OH	-	-	3563.2	3551.7
carbonates	1040.8	1040.8	1059.1	1053.3
Molar mass of X (g/mol)	35	80	127	17
Ionic radii of X^- (Å)	1.8	2	2.2	1.4

731

732

733

734

735

736

737

738

739

740

741

742

This is the peer-reviewed, final accepted version for American Mineralogist, published by the Mineralogical Society of America.
The published version is subject to change. Cite as Authors (Year) Title. American Mineralogist, in press.
DOI: https://doi.org/10.2138/am-2020-7452. http://www.minsocam.org/

743

744

745 Table 3. Measured, calculated, or extracted from the literature enthalpies of drop solution ΔH_{DS} in
746 $3Na_2O{\cdot}4MoO_3$ at 976 K, $\Delta H_{heat\ content\ (hc)}$ (for gases), and enthalpies of formation from elements
747 $\Delta H°_{f,el}$ used in thermochemical cycles for calculating $\Delta H°_{f,el}$ of the analyzed synthetic analogs of
748 mimetite.

Compound	ΔH_{DS} or ΔH_{hc} (g, 700 °C) (kJ/mol)	$\Delta H°_{f,\ el}$ (kJ/mol)
$Pb_{5.00}(AsO_4)_{3.00}Cl_{0.80}(CO_3)_{0.10}$	533.38 ± 13.75*	-3026.6 ± 15.8*
$Pb_{5.00}\ (AsO_4)_{3.00}Br_{0.80}(CO_3)_{0.10}$	514.23 ± 22.40*	-2967.6 ± 25.0*
$Pb_{5.00}\ (AsO_4)_{3.00}I_{0.45}OH_{0.35}(CO_3)_{0.10}$	498.96 ± 8.34*	-2993.1 ± 12.2*
$Pb_{5.00}\ (AsO_4)_{3.00}OH_{0.86}(CO_3)_{0.07}$	474.66 ± 9.79*	-3030.6 ± 11.5*
PbO	-15.39 ± 1.14[a]	-217.3 ± 0.3[c]
As_2O_5	76.70 ± 0.80[b]	-926.0[d]
K_2O	-318.00 ± 3.10[e]	-363.2 ± 2.1[c]
KCl	71.32 ± 1.38*	-436.5 ± 0.2[c]
KBr	78.41 ± 2.01*	-393.8 ± 0.2[c]
I_2(g)	87.85[f]	0
Br_2(g)	56.09[f]	0
CO_2(g)	32.07[f]	-393.5 ± 1.3[c]
H_2O(g)	69.00[c]	-285.8 ± 0.1[c]
O_2(g)	21.74[c]	0

This is the peer-reviewed, final accepted version for American Mineralogist, published by the Mineralogical Society of America.
The published version is subject to change. Cite as Authors (Year) Title. American Mineralogist, in press.
DOI: https://doi.org/10.2138/am-2020-7452. http://www.minsocam.org/

749 Note: g - gas; the uncertainty represents two standard deviations of the mean ($2\sigma_M$); * - this work
750 (see Supplemental[1] Tables S1–S6); [a] - Majzlan et al. (2002); [b] - Forray et al. (2014); [c] - Robie and
751 Hemingway (1995); [d] - Dinsdale (1991); [e] - Navrotsky (2014); [f] - calculated from JANAF.
752
753 Table 4. Reactions and thermodynamic cycles used for $Pb_5(AsO_4)_3OH_{0.86}(CO_3)_{0.07}$ to calculate
754 the enthalpy of formation from the elements at 25 °C according to the reaction: $5PbO + 1.5As_2O_5$
755 $+ 0.43H_2O + 0.07CO_2 = Pb_{5.00}(AsO_4)_{3.00}OH_{0.86}(CO_3)_{0.07}$.

No	Reaction	ΔH (kJ/mol)
(1)	$Pb_{5.00}(AsO_4)_{3.00}OH_{0.86}(CO_3)_{0.07(c,\ 25\ °C)} \rightarrow 5PbO_{(sln,\ 700\ °C)} + 1.5As_2O_{5(sln,\ 700\ °C)} + 0.43H_2O_{(g,\ 700\ °C)} + 0.07CO_{2(g,\ 700\ °C)}$	$\Delta H_{(1)} = \Delta H_{DS}[Pb_{5.00}(AsO_4)_{3.00}OH_{0.86}(CO_3)_{0.07}]$
(2)	$PbO_{(c,\ 25\ °C)} \rightarrow PbO_{(sln,\ 700\ °C)}$	$\Delta H_{(2)} = \Delta H_{DS}(PbO)$[a]
(3)	$As_2O_{5(c,\ 25\ °C)} \rightarrow As_2O_{5(sln,\ 700\ °C)}$	$\Delta H_{(3)} = \Delta H_{DS}(As_2O_5)$[b]
(4)	$H_2O_{(l,\ 25\ °C)} \rightarrow H_2O_{(g,\ 700\ °C)}$	$\Delta H_{(4)} = \Delta H_{hc}(H_2O)$[c]
(5)	$CO_{2(g,\ 25\ °C)} \rightarrow CO_{2(g,\ 700\ °C)}$	$\Delta H_{(5)} = \Delta H_{hc}(CO_2)$[d]
(6)	$Pb_{(c,\ 25\ °C)} + 0.5O_{2(g,\ 25\ °C)} \rightarrow PbO_{(c,\ 25\ °C)}$	$\Delta H_{(6)} = \Delta H_{f,\ el}(PbO)$[c]
(7)	$2As_{(c,\ 25\ °C)} + 2.5O_{2(g,\ 25\ °C)} \rightarrow As_2O_{5(c,\ 25\ °C)}$	$\Delta H_{(7)} = \Delta H_{f,\ el}(As_2O_5)$[e]
(8)	$H_{2(g,\ 25\ °C)} + 0.5O_{2(g,\ 25\ °C)} \rightarrow H_2O_{(l,\ 25\ °C)}$	$\Delta H_{(8)} = \Delta H_{f,\ el}(H_2O)$[c]
(9)	$C_{(c,\ 25\ °C)} + O_{2(g,\ 25\ °C)} \rightarrow CO_{2(g,\ 25\ °C)}$	$\Delta H_{(9)} = \Delta H_{f,\ el}(CO_2)$[c]
(10)	$5Pb_{(c,\ 25\ °C)} + 3As_{(c,\ 25\ °C)} + 0.43H_{2(g,\ 25\ °C)} + 6.535O_{2(g,\ 25\ °C)} + 0.07C_{(c,\ 25\ °C)} \rightarrow Pb_{5.00}(AsO_4)_{3.00}OH_{0.86}(CO_3)_{0.07\ (c,\ 25\ °C)}$	$\Delta H_{(10)} = \Delta H_{f,\ el}[Pb_{5.00}(AsO_4)_{3.00}OH_{0.86}(CO_3)_{0.07}] = -\Delta H_{(1)} + 5\Delta H_{(2)} + 1.5\Delta H_{(3)} + 0.43\Delta H_{(4)} + 0.07\Delta H_{(5)} + 5\Delta H_{(6)} + 1.5\Delta H_{(7)} + 0.43\Delta H_{(8)}$

This is the peer-reviewed, final accepted version for American Mineralogist, published by the Mineralogical Society of America.
The published version is subject to change. Cite as Authors (Year) Title. American Mineralogist, in press.
DOI: https://doi.org/10.2138/am-2020-7452. http://www.minsocam.org/

		$+ 0.07\Delta H_{(9)}$

Note: c - crystal; sln - solution; g - gas; l - liquid; [a] - Majzlan et al. (2002); [b] - Forray et al. (2014); [c] - Robie and Hemingway (1995); [d] - calculated from JANAF; [e] - Dinsdale (1991).

Table 5. Reactions and thermodynamic cycles used for $Pb_{5.00}(AsO_4)_{3.00}Cl_{0.80}(CO_3)_{0.10}$ to calculate the enthalpies of formation from the elements at 25 °C according to the reaction: $5PbO + 1.5As_2O_5 + 0.8KCl + 0.1CO_2 = Pb_{5.00}(AsO_4)_{3.00}Cl_{0.80}(CO_3)_{0.10} + 0.4K_2O$.

No	Reaction	ΔH (kJ/mol)
(1)	$Pb_{5.00}(AsO_4)_{3.00}Cl_{0.80}(CO_3)_{0.10(c,\ 25\ °C)} + 0.4K_2O_{(c,\ 25\ °C)} \rightarrow 5PbO_{(sln,\ 700\ °C)} + 1.5As_2O_{5(sln,\ 700\ °C)} + 0.8KCl_{(sln,\ 700\ °C)} + 0.1CO_{2(g,\ 700°C)}$	$\Delta H_{(1)} = \Delta H_{DS}[Pb_{5.00}(AsO_4)_{3.00}Cl_{0.80}(CO_3)_{0.10}] + 0.4\Delta H_{DS}(K_2O)$
(2)	$PbO_{(c,\ 25\ °C)} \rightarrow PbO_{(sln,\ 700\ °C)}$	$\Delta H_{(2)} = \Delta H_{DS}(PbO)$[a]
(3)	$As_2O_{5(c,\ 25\ °C)} \rightarrow As_2O_{5(sln,\ 700\ °C)}$	$\Delta H_{(3)} = \Delta H_{DS}(As_2O_5)$[b]
(4)	$KCl_{(c,\ 25\ °C)} \rightarrow KCl_{(sln,\ 700\ °C)}$	$\Delta H_{(4)} = \Delta H_{DS}(KCl)$*
(5)	$K_2O_{(c\ 25\ °C)} \rightarrow K_2O_{(sln,\ 700\ °C)}$	$\Delta H_{(5)} = \Delta H_{DS}(K_2O)$[c]
(6)	$CO_{2(g,\ 25\ °C)} \rightarrow CO_{2(g,\ 700\ °C)}$	$\Delta H_{(5)} = \Delta H_{hc}(CO_2)$[d]
(7)	$Pb_{(c,\ 25\ °C)} + 0.5O_{2(g,\ 25\ °C)} \rightarrow PbO_{(c,\ 25\ °C)}$	$\Delta H_{(7)} = \Delta H_{f,\ el}(PbO)$[e]
(8)	$2As_{(c,\ 25\ °C)} + 2.5O_{2(g,\ 25\ °C)} \rightarrow As_2O_{5(c,\ 25\ °C)}$	$\Delta H_{(8)} = \Delta H_{f,\ el}(As_2O_5)$[f]
(9)	$K_{(c,\ 25\ °C)} + 0.5Cl_{2(g,\ 25\ °C)} \rightarrow KCl_{(c,\ 25\ °C)}$	$\Delta H_{(9)} = \Delta H_{f,\ el}(KCl)$[e]
(10)	$2K_{(c,\ 25\ °C)} + 0.5O_{2(g,\ 25\ °C)} \rightarrow K_2O_{(\ 25\ °C)}$	$\Delta H_{(10)} = \Delta H_{f,\ el}(K_2O)$[e]
(11)	$C_{(c,\ 25\ °C)} + O_{2(g,\ 25\ °C)} \rightarrow CO_{2(g,\ 25\ °C)}$	$\Delta H_{(11)} = \Delta H_{f,\ el}(CO_2)$[e]
(12)	$5Pb_{(c,\ 25\ °C)} + 3As_{(c,\ 25\ °C)} + 0.4Cl_{2(g,\ 25\ °C)} + 0.1C_{(c,\ 25\ °C)} + 6.15O_{2(g,\ 25\ °C)} \rightarrow$	$\Delta H_{(12)} = \Delta H_{f,\ el}[Pb_{5.00}(AsO_4)_{3.00}Cl_{0.80}(CO_3)_{0.10}] = -\Delta H_{(1)} +$

This is the peer-reviewed, final accepted version for American Mineralogist, published by the Mineralogical Society of America.
The published version is subject to change. Cite as Authors (Year) Title. American Mineralogist, in press.
DOI: https://doi.org/10.2138/am-2020-7452. http://www.minsocam.org/

$Pb_{5.00}(AsO_4)_{3.00}Cl_{0.80}(CO_3)_{0.10(c,\ 25\ °C)}$	$5\Delta H_{(2)} + 1.5\Delta H_{(3)} + 0.8\Delta H_{(4)} + 0.1\Delta H_{(6)} + 5\Delta H_{(7)} + 1.5\Delta H_{(8)} + 0.8\Delta H_{(9)} + 0.1\Delta H_{(11)} - 0.4\Delta H_{(10)}$

Note: c - crystal; sln - solution; g - gas; * - This work (see Supplemental[1] Table S5); [a] - Majzlan et al. (2002); [b] - Forray et al. (2014); c - Navrotsky (2014); [d] - calculated from JANAF; [e] - Robie and Hemingway (1995); [f] - Dinsdale (1991).

This is the peer-reviewed, final accepted version for American Mineralogist, published by the Mineralogical Society of America.
The published version is subject to change. Cite as Authors (Year) Title. American Mineralogist, in press.
DOI: https://doi.org/10.2138/am-2020-7452. http://www.minsocam.org/

783

784 Table 6. Reactions and thermodynamic cycles used for $Pb_{5.00}(AsO_4)_{3.00}Br_{0.80}(CO_3)_{0.10}$ to calculate
785 the enthalpies of formation from the elements at 25 °C according to the reaction: $5PbO + 1.5As_2O_5 + 0.8KBr + 0.1CO_2 = Pb_{5.00}(AsO_4)_{3.00}Br_{0.80}(CO_3)_{0.10} + 0.4K_2O$.
786

No	Reaction	ΔH (kJ/mol)
(1)	$Pb_{5.00}(AsO_4)_{3.00}Br_{0.80}(CO_3)_{0.10(c,\ 25\ °C)} + 0.4K_2O_{(c,\ 25\ °C)} \rightarrow 5PbO_{(sln,\ 700\ °C)} + 1.5As_2O_{5(sln,\ 700\ °C)} + 0.8KBr_{(sln,\ 700\ °C)} + 0.1CO_{2(g,\ 700°C)}$	$\Delta H_{(1)} = \Delta H_{DS}[Pb_{5.00}(AsO_4)_{3.00}Br_{0.80}(CO_3)_{0.10}] + 0.4\Delta H_{DS}(K_2O)$
(2)	$PbO_{(c,\ 25\ °C)} \rightarrow PbO_{(sln,\ 700\ °C)}$	$\Delta H_{(2)} = \Delta H_{DS}(PbO)^a$
(3)	$As_2O_{5(c,\ 25\ °C)} \rightarrow As_2O_{5(sln,\ 700\ °C)}$	$\Delta H_{(3)} = \Delta H_{DS}(As_2O_5)^b$
(4)	$KBr_{(c,\ 25\ °C)} \rightarrow KBr_{(sln,\ 700\ °C)}$	$\Delta H_{(4)} = \Delta H_{DS}(KBr)^*$
(5)	$K_2O_{(c\ 25\ °C)} \rightarrow K_2O_{(sln,\ 700\ °C)}$	$\Delta H_{(5)} = \Delta H_{DS}(K_2O)^c$
(6)	$CO_{2(g,\ 25\ °C)} \rightarrow CO_{2(g,\ 700\ °C)}$	$\Delta H_{(6)} = \Delta H_{hc}(CO_2)^d$
(7)	$Pb_{(c,\ 25\ °C)} + 0.5O_{2(g,\ 25\ °C)} \rightarrow PbO_{(c,\ 25\ °C)}$	$\Delta H_{(7)} = \Delta H_{f,\ el}(PbO)^c$
(8)	$2As_{(c,\ 25\ °C)} + 2.5O_{2(g,\ 25\ °C)} \rightarrow As_2O_{5(c,\ 25\ °C)}$	$\Delta H_{(8)} = \Delta H_{f,\ el}(As_2O_5)^e$
(9)	$K_{(c,\ 25\ °C)} + 0.5Br_{2(g,\ 25\ °C)} \rightarrow KBr_{(c,\ 25\ °C)}$	$\Delta H_{(9)} = \Delta H_{f,\ el}(KBr)^c$
(10)	$2K_{(c,\ 25\ °C)} + 0.5O_{2(g,\ 25\ °C)} \rightarrow K_2O_{(\ 25\ °C)}$	$\Delta H_{(10)} = \Delta H_{f,\ el}(K_2O)^c$
(11)	$C_{(c,\ 25\ °C)} + O_{2(g,\ 25\ °C)} \rightarrow CO_{2(g,\ 25\ °C)}$	$\Delta H_{(11)} = \Delta H_{f,\ el}(CO_2)^c$
(12)	$5Pb_{(c,\ 25\ °C)} + 3As_{(c,\ 25\ °C)} + 0.4Br_{2(g,\ 25\ °C)} + 0.1C_{(c,\ 25\ °C)} + 6.075O_{2(g,\ 25\ °C)} \rightarrow Pb_{5.00}(AsO_4)_{3.00}Br_{0.80}(CO_3)_{0.10\ (c,\ 25\ °C)}$	$\Delta H_{(12)} = \Delta H_{f,\ el}[Pb_{5.00}(AsO_4)_{3.00}Br_{0.80}(CO_3)_{0.10}] = -\Delta H_{(1)} + 5\Delta H_{(2)} + 1.5\Delta H_{(3)} + 0.8\Delta H_{(4)} + 0.1\Delta H_{(6)} + 5\Delta H_{(7)} + 1.5\Delta H_{(8)} + 0.8\Delta H_{(9)} + 0.1\Delta H_{(11)} - 0.4\Delta H_{(10)}$

Note: c - crystal; sln - solution; g - gas; * - This work (see Supplemental[1] Table S6); [a] – Majzlan et al. 2002; [b] - Forray et al. (2014); [c] – Robie and Hemingway (1995); [d] - calculated from JANAF; [e] - Dinsdale (1991).

This is the peer-reviewed, final accepted version for American Mineralogist, published by the Mineralogical Society of America.
The published version is subject to change. Cite as Authors (Year) Title. American Mineralogist, in press.
DOI: https://doi.org/10.2138/am-2020-7452. http://www.minsocam.org/

Table 7. Reactions and thermodynamic cycles used for $Pb_{5.00}(AsO_4)_{3.00}I_{0.45}OH_{0.35}(CO_3)_{0.10}$ to calculate the enthalpies of formation from the elements at 25 °C according to the reaction: $5PbO + 1.5As_2O_5 + 0.225I_2 + 0.175H_2O + 0.1CO_2 = Pb_{5.00}(AsO_4)_{3.00}I_{0.45}OH_{0.35}(CO_3)_{0.10} + 0.1125O_2$.

No	Reaction	ΔH (kJ/mol)
(1)	$Pb_{5.00}(AsO_4)_{3.00}I_{0.45}OH_{0.35}(CO_3)_{0.10(c,\ 25\ °C)} + 0.1125O_{2(g,\ 25\ °C)} \rightarrow 5PbO_{(sln,\ 700\ °C)} + 1.5As_2O_{5(sln,\ 700\ °C)} + 0.225I_{2(g,\ 700\ °C)} + 0.175H_2O_{(g,\ 700°C)} + 0.1CO_{2(g,\ 700°C)}$	$\Delta H_{(1)} = \Delta H_{DS}[Pb_{5.00}(AsO_4)_{3.00}I_{0.45}OH_{0.35}(CO_3)_{0.10}] + 0.1125\Delta H_{hc}(O_2)$
(2)	$PbO_{(c,\ 25\ °C)} \rightarrow PbO_{(sln,\ 700\ °C)}$	$\Delta H_{(2)} = \Delta H_{DS}(PbO)^a$
(3)	$As_2O_{5(c,\ 25\ °C)} \rightarrow As_2O_{5(sln,\ 700\ °C)}$	$\Delta H_{(3)} = \Delta H_{DS}(As_2O_5)^b$
(4)	$I_{2(s,\ 25\ °C)} \rightarrow I_{2(g,\ 700\ °C)}$	$\Delta H_{(4)} = \Delta H_{hc}(I_2)^c$
(5)	$H_2O_{(l,\ 25\ °C)} \rightarrow H_2O_{(g,\ 700\ °C)}$	$\Delta H_{(5)} = \Delta H_{hc}(H_2O)^d$
(6)	$CO_{2(g,\ 25\ °C)} \rightarrow CO_{2(g,\ 700\ °C)}$	$\Delta H_{(6)} = \Delta H_{hc}(CO_2)^c$
(7)	$O_{2(g,\ 25\ °C)} \rightarrow O_{2(g,\ 700\ °C)}$	$\Delta H_{(7)} = \Delta H_{hc}(O_2)^d$
(8)	$Pb_{(c,\ 25\ °C)} + 0.5O_{2(g,\ 25\ °C)} \rightarrow PbO_{(c,\ 25\ °C)}$	$\Delta H_{(8)} = \Delta H_{f,\ el}(PbO)^d$
(9)	$2As_{(c,\ 25\ °C)} + 2.5O_{2(g,\ 25\ °C)} \rightarrow As_2O_{5(c,\ 25\ °C)}$	$\Delta H_{(9)} = \Delta H_{f,\ el}(As_2O_5)^e$
(10)	$H_{2(g,\ 25\ °C)} + 0.5O_{2(g,\ 25\ °C)} \rightarrow H_2O_{(l,\ 25\ °C)}$	$\Delta H_{(10)} = \Delta H_{f,\ el}(H_2O)^d$
(11)	$C_{(c,\ 25\ °C)} + O_{2(g,\ 25\ °C)} \rightarrow CO_{2(g,\ 25\ °C)}$	$\Delta H_{(11)} = \Delta H_{f,\ el}(CO_2)^d$
(12)	$5Pb_{(c,\ 25\ °C)} + 3As_{(c,\ 25\ °C)} + 0.225I_{2(s,\ 25\ °C)} + 0.175H_{2(g,\ 25\ °C)} + 0.1C_{(c,\ 25\ °C)} + 6.325O_{2(g,\ 25\ °C)} \rightarrow Pb_{5.00}(AsO_4)_{3.00}I_{0.45}OH_{0.35}(CO_3)_{0.10\ (c,\ 25\ °C)}$	$\Delta H_{(12)} = \Delta H_{f,\ el}[Pb_{5.00}(AsO_4)_{3.00}I_{0.45}OH_{0.35}(CO_3)_{0.10}] = -\Delta H_{(1)} + 5\Delta H_{(2)} + 1.5\Delta H_{(3)} + 0.225\Delta H_{(4)} + 0.175\Delta H_{(5)} + 0.1\Delta H_{(6)} + 5\Delta H_{(8)} + 1.5\Delta H_{(9)} + 0.175\Delta H_{(10)} + 0.1\Delta H_{(11)}$

812 Note: sln - solution; g - gas; c - crystal; s - solid; l - liquid; [a] - Majzlan et al. (2002); [b] - Forray et
813 al. (2014); [c] - calculated from JANAF; [d] - Robie and Hemingway (1995); [e] - Dinsdale (1991).
814
815
816
817
818
819
820
821
822
823
824
825
826
827
828
829
830
831
832
833
834

This is the peer-reviewed, final accepted version for American Mineralogist, published by the Mineralogical Society of America.
The published version is subject to change. Cite as Authors (Year) Title. American Mineralogist, in press.
DOI: https://doi.org/10.2138/am-2020-7452. http://www.minsocam.org/

835 Table 8. Selected $\Delta H°_{f,\ el}$ of apatites extracted from Supplemental[1] Table S8 and other physical
836 and thermodynamic parameters of X (where X = F, OH, Cl, Br, and I) or binary compound MeX_2
837 (where Me = Ca and Pb) used for plotting diagrams in Figures 5 and 6.

Chemical formula of selected apatite-like phase:	$\Delta H°_{f,\ el}$ of apatite (kJ/mol)	Error (kJ/mol)	Molar mass (g/mol)	Ionic radius of X^- (Å)	I' - ionic character of Me-X bond	Pauling electronegativity χ_X of X	First ionisation energy E_X^+ of X (kJ/mol)	$\Delta H°_{f,\ el}$ of MeX_2 (cr.) (kJ/mol)
$Pb_5(AsO_4)_3F$	-	-	1471.8	1.33	1.17	3.98	1681	-676.0
$Pb_5(AsO_4)_3OH_{0.86}(CO_3)_{0.07}$	-3030.6	11.5	1471.6	1.40	0.89	3.51	1314	-516.0
$Pb_5(AsO_4)_3Cl_{0.80}(CO_3)_{0.10}$	-3026.6	15.8	1487.1	1.81	0.69	3.16	1252	-359.4
$Pb_5(AsO_4)_3Br_{0.80}(CO_3)_{0.10}$	-2967.6	25.0	1522.7	1.96	0.58	2.96	1140	-278.7
$Pb_5(AsO_4)_3I_{0.45}OH_{0.35}(CO_3)_{0.10}$	-2993.1	12.2	1521.8	2.20	0.42	2.66	1008	-175.2
$Ca_5(AsO_4)_3F$	-5639.3	42.8	636.1	1.33	1.68	3.98	1681	-1228.0
$Ca_5(AsO_4)_3OH$	-5604.0	41.0	634.2	1.40	1.38	3.51	1314	-986.1
$Ca_5(AsO_4)_3Cl$	-	-	652.6	1.81	1.16	3.16	1252	-795.4
$Ca_5(AsO_4)_3Br$	-	-	697.1	1.96	1.04	2.96	1140	-682.8
$Ca_5(AsO_4)_3I$	-	-	744.1	2.20	0.86	2.66	1008	-536.8
$Pb_5(PO_4)_3F$	-4233.0	31.5	1339.9	1.33	1.17	3.98	1681	-676.0
$Pb_5(PO_4)_3OH$	-4130.5	21.3	1337.9	1.40	0.89	3.51	1314	-516.0
$Pb_5(PO_4)_3Cl$	-4111.1	8.0	1356.4	1.81	0.69	3.16	1252	-359.4
$Pb_5(PO_4)_3Br$	-4090.0	-	1400.8	1.96	0.58	2.96	1140	-278.7
$Pb_5(PO_4)_3I$	-	-	1447.8	2.20	0.42	2.66	1008	-175.2

This is the peer-reviewed, final accepted version for American Mineralogist, published by the Mineralogical Society of America.
The published version is subject to change. Cite as Authors (Year) Title. American Mineralogist, in press.
DOI: https://doi.org/10.2138/am-2020-7452. http://www.minsocam.org/

$Ca_5(PO_4)_3F$	-6823.8	84.1	504.3	1.33	1.68	3.98	1681	-1228.0
$Ca_5(PO_4)_3OH$	-6710.5	75.7	502.3	1.40	1.38	3.51	1314	-986.1
$Ca_5(PO_4)_3Cl$	-6588.0	53.0	520.8	1.81	1.16	3.16	1252	-795.4
$Ca_5(PO_4)_3Br$	-6531.5	40.5	565.2	1.96	1.04	2.96	1140	-682.8
$Ca_5(PO_4)_3I$	-6474.5	16.0	612.2	2.20	0.86	2.66	1008	-536.8

Note: Ionic radius of X^- taken from Shannon and Prewitt (1969); I′ - ionic characteristic of Me-X bond as defined earlier by Dean (1999); χ_X of X extracted from Pauling (1988); first ionization energy E_X^+ of X taken from Dean (1999); $\Delta H°_{f,\,el}$ of MeX_2 (cr.) extracted from Robie and Hemingway (1995).

Table 9. Predicted $\Delta H°_{f,\,el}$ of apatite-like phases by the SSA model and lattice energies calculated based on the experimental volume V_m.

Chemical formula	arsenate	$\Delta H°_{f,\,el}$ (arsenate) (kJ/mol)	PbX_2	$\Delta H°_{f,\,el}$ (PbX_2) (kJ/mol)	$\Delta H°_{f,\,el}$ of apatite (SSA)	difference (SSA - exp)	% difference |(SSA - exp)/exp|	V_m (nm^3)	U_{POT} single cell (kJ)
$Pb_5(AsO_4)_3OH$	$Pb_3(AsO_4)_2$	-1780.2	$Pb(OH)_2$	-516.00	-2928.30	92.03	3.3%	0.338	18588
$Pb_5(AsO_4)_3Cl$	$Pb_3(AsO_4)_2$	-1780.2	$PbCl_2$	-359.41	-2850.01	156.87	4.0%	0.338	18591
$Pb_5(AsO_4)_3Br$	$Pb_3(AsO_4)_2$	-1780.2	$PbBr_2$	-278.65	-2809.63	138.90	5.3%	0.344	18697
$Pb_5(AsO_4)_3I$	$Pb_3(AsO_4)_2$	-1780.2	PbI_2	-175.20	-2757.90	205.84	7.8%	0.350	18794

Note: $\Delta H°_{f,\,el}$ for arsenate and PbX_2 (where X = OH, Cl, Br, and I) are taken from Robie and Hemingway (1995); SSA - simple salt approximation; exp - experimental value; V_m - experimental molar volume of a unit cell (Sordyl et al. 2020); U_{POT} - lattice energy.

Figure 1.

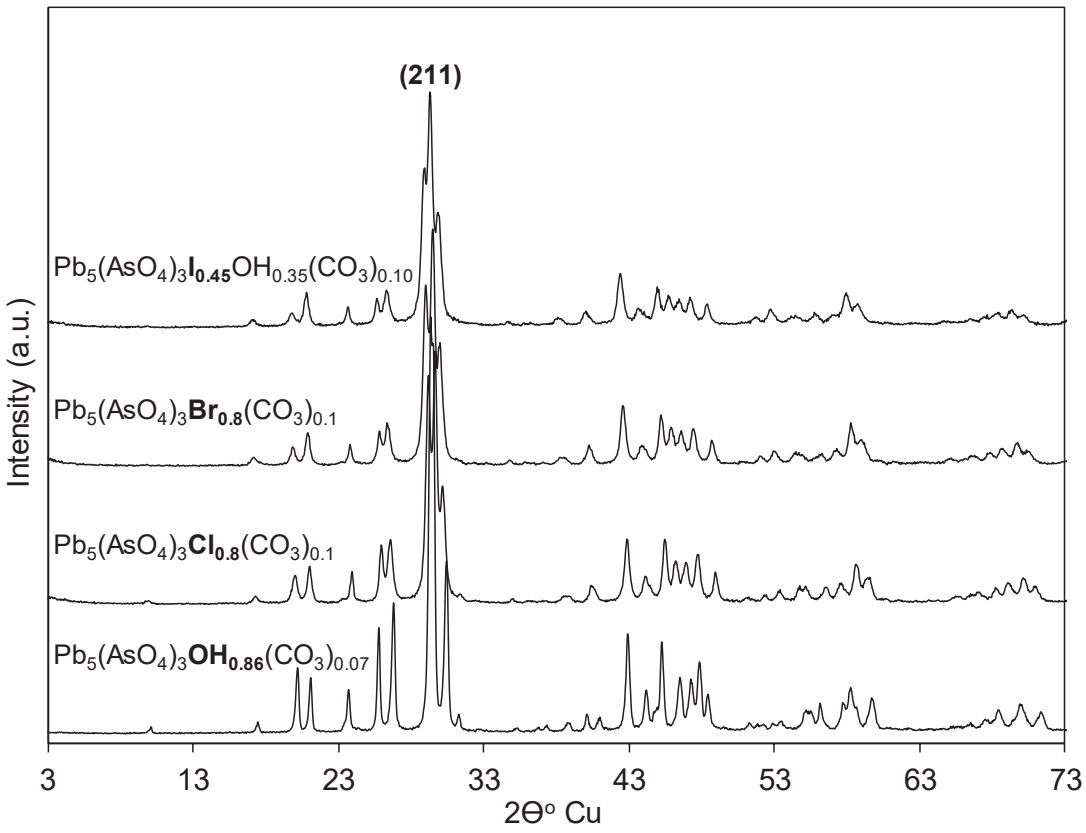

This is the peer-reviewed, final accepted version for American Mineralogist, published by the Mineralogical Society of America.
The published version is subject to change. Cite as Authors (Year) Title. American Mineralogist, in press.
DOI: https://doi.org/10.2138/am-2020-7452. http://www.minsocam.org/

Figure 2.

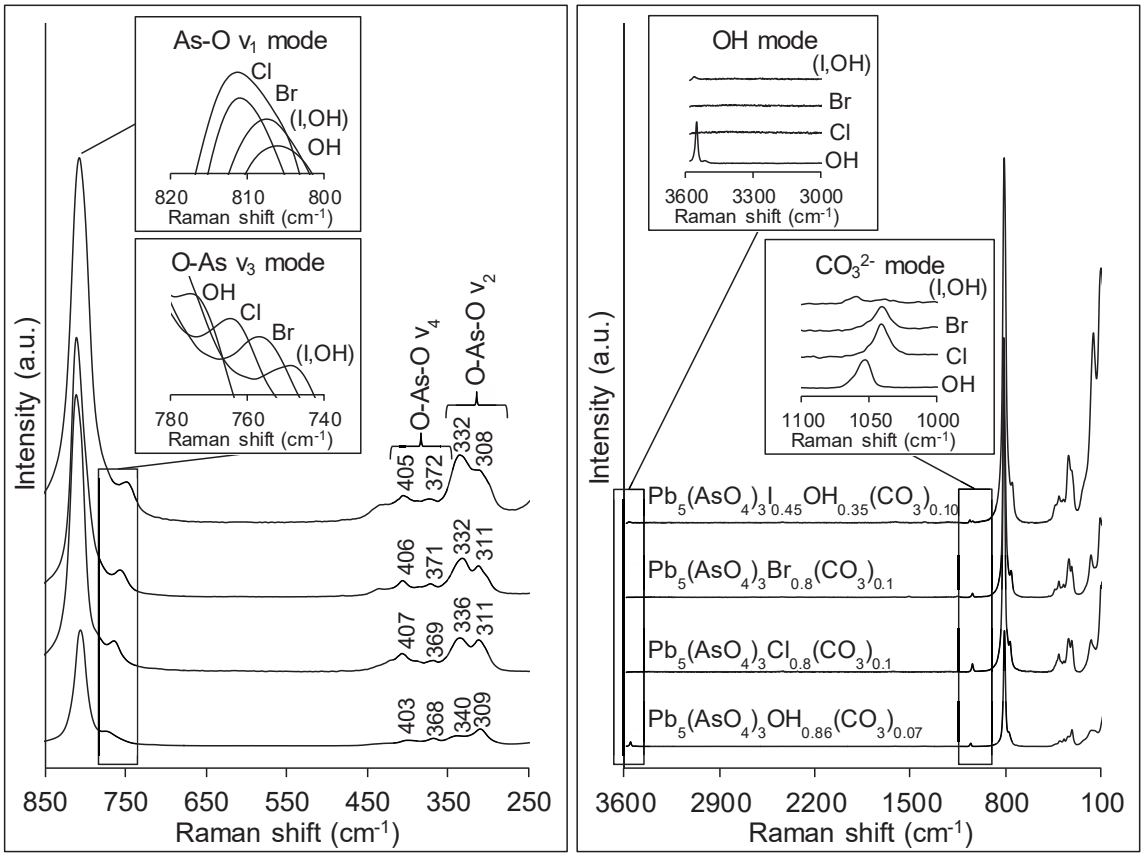

Figure 3.

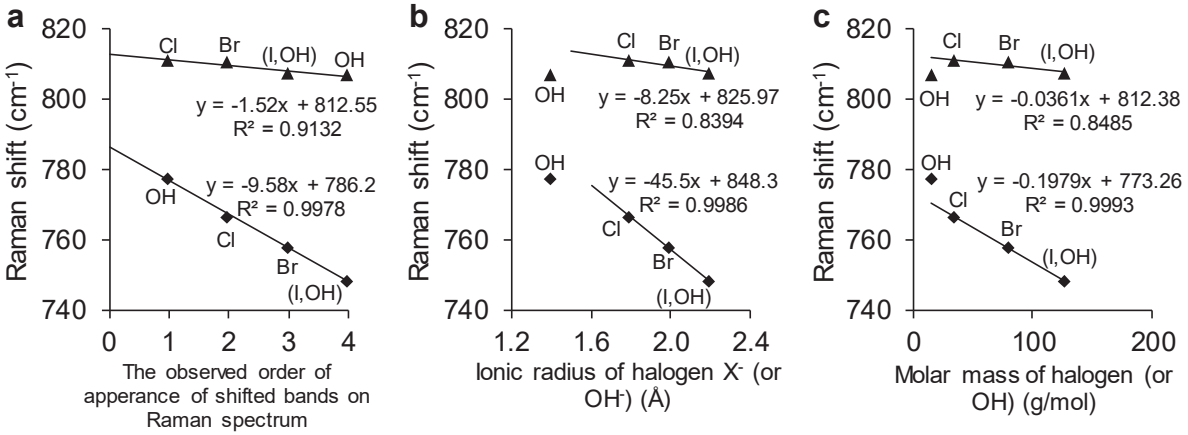

This is the peer-reviewed, final accepted version for American Mineralogist, published by the Mineralogical Society of America.
The published version is subject to change. Cite as Authors (Year) Title. American Mineralogist, in press.
DOI: https://doi.org/10.2138/am-2020-7452. http://www.minsocam.org/

Figure 4.

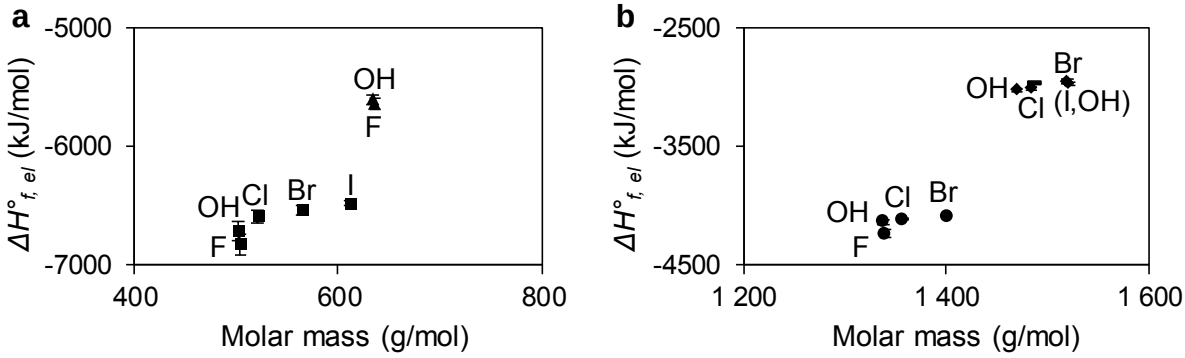

This is the peer-reviewed, final accepted version for American Mineralogist, published by the Mineralogical Society of America.
The published version is subject to change. Cite as Authors (Year) Title. American Mineralogist, in press.
DOI: https://doi.org/10.2138/am-2020-7452. http://www.minsocam.org/

Figure 5.

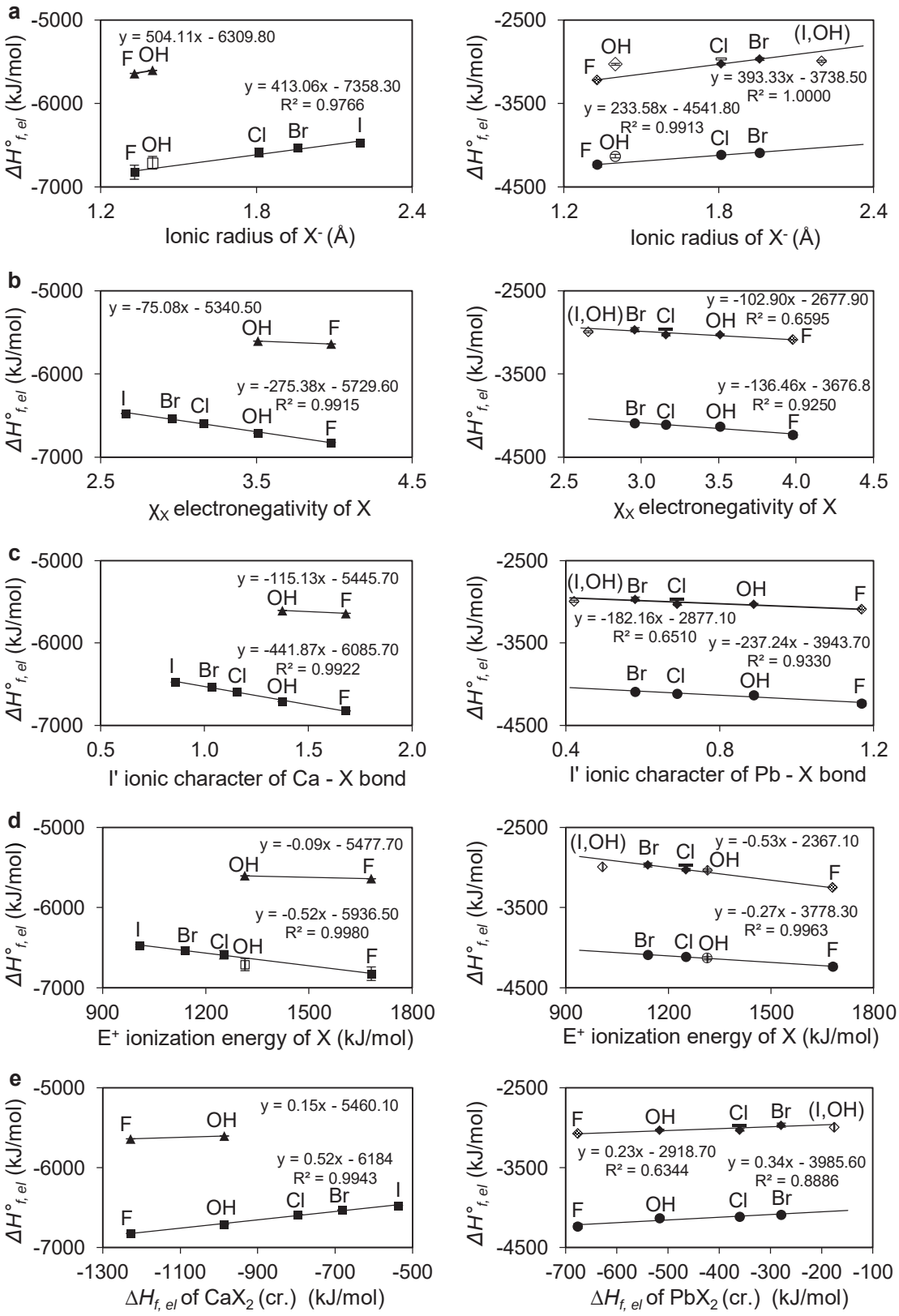

This is the peer-reviewed, final accepted version for American Mineralogist, published by the Mineralogical Society of America.
The published version is subject to change. Cite as Authors (Year) Title. American Mineralogist, in press.
DOI: https://doi.org/10.2138/am-2020-7452. http://www.minsocam.org/

Figure 6.